Solvent effects in the liquid phase hydrodeoxygenation of methyl propionate over a Pd(111) catalyst model

Sina Behtash, Jianmin Lu, Eric Walker, Osman Mamun, and Andreas Heyden*

Department of Chemical Engineering, University of South Carolina,

301 S. Main St., Columbia, South Carolina 29208, USA

*Corresponding author: email: heyden@cec.sc.edu

Abstract

Solvation effects of liquid water and 1,4-dioxane have been studied from first principles for the hydrodeoxygenation of methyl propionate over a Pd (111) catalyst surface model. Microkinetic reaction models have been developed for various reaction environments to study the effects of solvents on the reaction mechanism. Our models predict that in all reaction environments, decarbonylation pathways are favored over decarboxylation pathways. However, in the presence of liquid water the decarboxylation mechanism is facilitated due to solvent stabilization of the dehydrogenated derivatives of propionate. Overall, the activity of Pd (111) is one order of magnitude lower in water than in 1,4-dioxane where we predict the activity to be very similar to the vapor phase. The decrease in Pd (111) activity due to liquid water can be traced back to the Pd surface being more crowded and propanoyl-methoxy type dissociations becoming more difficult. Propanoyl-methoxy type dissociations also become more rate controlling in liquid water than the dehydrogenation steps that are most rate controlling in 1,4-dioxane and in the vapor phase.

Keywords:

Solvent effects; organic esters; methyl propionate; palladium; density functional theory; COSMO; decarbonylation; decarboxylation; microkinetic modeling

1. Introduction

Lipid-rich biomass such as vegetable oils, waste fats, and algal lipids constitute an important class of raw materials for the production of green fuels. These lipid feedstocks contain primarily oxygenates such as triglycerides and fatty acids. The conversion of these molecules to liquid hydrocarbon molecules has been investigated using hydrotreatment processes and conventional hydrodesulphurization catalysts such as sulfided $NiMo/Al_2O_3$ and $CoMo/Al_2O_3$.[1-3] However, considering the low level of sulfur in biomass and the higher activity of oxygenated feeds versus sulfided feedstocks, conventional hydrotreatment catalysts have been found to display a short catalyst lifetime. In our quest to rationally design a transition metal catalyst for the hydrodeoxygenation (HDO) of fatty acids and esters, we have previously investigated the kinetics and reaction mechanism of the HDO of propionic acid[4-5] and methyl propionate[6] over metal catalysts under gas-phase conditions. We purposefully selected propionic acid and methyl propionate as a model organic acid and ester molecule since they are small enough to be modeled efficiently from first principles, they can be studied experimentally in both vapor and liquid phase environments, and they can form a C=C double bond between the C_α and C_β atoms of the parent organic acid/ester required for a keto-enol tautomerism that has been observed during the HDO of methyl laurate by Donnis et al.[2] However, as industrial hydrotreatment processes often occur in a complex liquid environment, our understanding of the mechanism cannot be completed without studying the solvent effects on the kinetics of the HDO of organic acids and esters.

Solvent effects in heterogeneous catalysis have been rationalized by correlating reaction rates and product distributions with the polarity or dielectric constant and activity coefficients.[7-10] It has been observed that a polar solvent often enhances the adsorption of the non-polar reactant,

while a non-polar solvent enhances the adsorption of a polar reactant.[10-13] For example in the competitive hydrogenation of acetone and cyclohexene, polar solvents enhanced the reaction rate of the conversion of cyclohexene to cyclohexane while it reduced the adsorption of acetone.[11-12] A similar behavior has also been reported for the hydrogenation of 1-hexene and 2-methyl-3-buten-2-ol over silica supported Pt[13] and the hydrogenation of *o*-nitrotolene where the authors[14] were able to correlate the reaction rates with the activity coefficients.

While solvent polarity can qualitatively explain the changes in the kinetics of reactions or product distributions, more work remains to be done to explain and characterize the solvent effects quantitatively. With recent developments in the application of density functional theory for characterization of the properties of molecules at heterogeneous interfaces, a better understanding of the interaction of solvents, reaction intermediates, and a catalyst surface is obtainable. The effects of solvents on the reaction parameters of elementary reactions in a chemical process can be quantified using various solvation models such as implicit, explicit or hybrid explicit and implicit solvation models.[15-21] We developed recently a highly efficient implicit solvation scheme for metal surfaces (*iSMS*)[16] and applied it to the investigation of solvent effects in the HDO of propionic acid over Pd catalysts.[22-23] The key advantage of our *iSMS* methodology is that it permits the use of previously parameterized temperature dependent implicit solvation models from the homogeneous and enzyme catalysis communities for the computation of reaction free energies of elementary reactions at "periodic" metal surfaces described by plane wave density functional theory (DFT). Consequently, we reap the benefits of decades of experience with these solvation models and we are able to study the approximate effect of a solvent on elementary reaction rates of processes occurring at a solid-liquid interface under biomass processing conditions (~200°C and high pressure). In addition, rapid *in silico*

solvent screening for the rational design of solvents or even solvent mixtures for heterogeneous metal catalysis applications is within reach.

In our previous study, we found that non-polar solvents such as octane do not change the kinetics of the HDO of propionic acid, while polar solvents such as water can influence the kinetics and reaction mechanism. For example, in liquid water the overall activity was enhanced by one order of magnitude and the turnover frequency of the decarboxylation pathway, which is not favored under gas-phase conditions, was increased by 2-3 orders of magnitudes, such that the decarboxylation became competitive to the decarbonylation mechanism (which is the dominant mechanism under gas-phase conditions).[22-23] We note that in these simulations the fugacity/activity of all reactants and products have been equivalent in all reaction environments, i.e., the driving force for reaction is equivalent in all systems and the acceleration of the various reaction pathways originates exclusively from a change in the free energy profiles of the surface reactions caused by the solvent.

In this study, we extend our previous investigation to solvent effects on the HDO of organic esters such as methyl propionate over Pd (111) surface sites. In particular, we study the effects of the presence of liquid water and 1,4-dioxane which are typical protic and aprotic polar solvents. We focus on Pd (111) surface sites since Pd catalysts have previously been studied by us experimentally and computationally and are generally known to be quite active for the HDO of organic ester and acids.[4-6, 23-26] Also, we identified the (111) surface to be the main active site for the HDO of organic acids over Pd/C catalysts.[25] After investigating the effect of these solvents on the free energies of all elementary steps in the reaction mechanism, we developed a mean-field microkinetic model to study the effects of these solvents on the overall reaction kinetics and mechanism of the HDO of methyl propionate.

2. Methods

2.1 Solvation Model

The approximate effect of a solvent is investigated with the help of the *iSMS* method.[16] More information about *iSMS* and a validation of this methodology has recently been published.[16] Also, an explicit (QM/MM) solvation model for metal surfaces (*eSMS*) with TIP3P water molecules has yielded similar results to *iSMS* for C-C bond cleavage in dehydrogenated ethylene glycol over Pt(111) which further validates the accuracy of *iSMS* (the solvation effect on the reaction free energy and activation free energy was computed to be +0.11 and +0.11 eV by *iSMS* and +0.10 and +0.21 eV by *eSMS*, respectively).[21] Nevertheless, a limitation of all implicit solvation models remains that solvent coordinates are not part of the reaction coordinate which leads generally to an overestimation of reaction barriers. However, considering the accuracy of DFT (or lack thereof) in predicting activation barriers[27], we consider these effects to be most likely of minor importance. Also, we refrained from using a microsolvation approach[28] due to the difficulty in placing the solvent molecules for such a large number of elementary reaction steps investigated in this study.

The key idea of *iSMS* is to include the long-range metal interactions through periodic-slab calculations within the framework of DFT calculations in the absence of a solvent and to consider the effect of the liquid as a localized perturbation (small or large) of free-energy differences that can be described by cluster models embedded in an implicit solvent. Specifically, we define a free-energy function for an adsorbed intermediate on a periodic metal slab at the solid-liquid interface, $G^{liquid}_{surface+intermediate}$, using a simple subtraction scheme (similar in spirit to the ONIOM method[29] and the approach by Goddard et al.[30]):

$$G^{liquid}_{surface+intermediate} = G^{vacuum}_{surface+intermediate} + (G^{liquid}_{cluster+intermediate} - E^{vacuum}_{cluster+intermediate}) \quad (1)$$

where, $G^{vacuum}_{surface+intermediate}$, is the free energy in the absence of a solvent (plane-wave DFT energy of the periodic slab model including vibrational contributions to the free energy), $G^{liquid}_{cluster+intermediate}$ is the free energy of a metal cluster in the liquid (without explicitly considering vibrational contributions) constructed by removing selected metal atoms from the periodic-slab model and removing the periodic boundary conditions, and $E^{vacuum}_{cluster+intermediate}$ is the DFT energy of the same cluster in the absence of the solvent. We used the COSMO-RS[31-32] implicit solvation model to compute $G^{liquid}_{cluster+intermediate}$. COSMO-RS calculations have been performed using the COSMOtherm program.[33] Thermodynamic properties of the solvents are obtained from the COSMOtherm database, based on the results of quantum chemical COSMO calculations at the BP-TZVP level of theory. For all other structures, COSMO-RS input files have been generated from the COSMO calculations at the same level of theory.

2.2 DFT calculations

Cluster model DFT calculations were carried out using TURBOMOLE 6.0.[34-36] The Pd(111) cluster surfaces have been modeled by a two layered cluster with a 5×5 surface. These structures were constructed by removal of the periodic boundaries from the periodic slabs that were obtained from our previous plane-wave (VASP)[37-38] calculations.[5] In the supporting information, we present a convergence test that suggests reasonably converged results with cluster size have been obtained. Specifically, Figures S1 and S2 show that converged results have been obtained to about 0.15 kcal/mol. Overall, we believe our approach is converged to at least 1 kcal/mol, where the largest deviations occur for surface species such as F* and OH* (here, more metal layers are preferred). None of these species play any role in the investigated

reaction mechanism. Next, we note that the beta phase of Pd hydride is not thermodynamically stable at our reaction conditions of 473 K as long as the hydrogen partial pressure does not exceed 3 bar.[39] Considering that the hydrogen partial pressure in this study is 0.2 bar, it is reasonable to assume that also no beta hydride surface phase is present under these reaction conditions.

All adsorbates were represented by all-electron TZVP[40-42] basis sets while for Pd we used a relativistic small core potential (ECP) together with a basis set of same quality as the adsorbates for the valence electrons. The Coulomb potential was approximated with the RI-J approximation with auxiliary basis sets.[43-45] Single point energy calculations were performed with a self-consistent field energy convergence criterion of 1.0×10^{-6}. Finally, for each cluster model, energy calculations on various spin surfaces were performed to identify the lowest energy spin state for inclusion in equation 1. For cluster models in the liquid phase, COSMO calculations were performed on the same spin surface as for the vacuum cluster calculations. The dielectric constant was set to infinity as required for COSMO-RS calculations. Default radii-based cavities were used for cavity construction. Radii are listed in the supporting information.

2.3 Microkinetic Modeling

For surface reactions, the forward rate constant (k_{for}) of each reaction was calculated as

$$k_{for} = \frac{k_B T}{h} e^{-\frac{\Delta G^{\ddagger}}{k_B T}} \qquad (2)$$

where k_B is the Boltzmann constant, T denotes the reaction temperature, h is the Planck constant, and $\Delta G^{\ddagger}$ represents the free energy of activation for a specific temperature and reaction environment. In the presence of solvents, the free energy of activation ($\Delta G^{\ddagger}_{solvent}$) and the free energy of reaction ($\Delta G_{rxn\text{-}solvent}$) were calculated as,

$$\Delta G^{\ddagger}_{\text{Solvent}} = \Delta G^{\ddagger}_{\text{Gas}} + G_{TS}(solv) - G_{IS}(solv), \quad (3)$$

and

$$\Delta G_{\text{rxn-solvent}} = \Delta G_{\text{Gas}} + G_{FS}(solv) - G_{IS}(solv) \quad (4)$$

where, $G_{IS}(solv)$, $G_{FS}(solv)$, and $G_{TS}(solv)$ are the solvation free energies of the initial, final, and transition states, respectively, that were obtained from the difference in energy of the COSMO-RS and gas-phase cluster calculations, and $\Delta G^{\ddagger}_{\text{Gas}}$ and ΔG_{Gas} are the free energies of activation and reaction under gas phase conditions, respectively. The reverse rate constant (k_{rev}) is calculated from the thermodynamic equilibrium constant K

$$k_{\text{rev}} = \frac{k_{\text{for}}}{K} \quad (5)$$

For an adsorption reaction, A(g)+*→A*, the rate of adsorption is given by collision theory with a sticking probability of 1 independent of solvent

$$k_{\text{for}} = \frac{1}{N_0\sqrt{2\pi m_A k_B T}} \quad (6)$$

where N_0 is the number of sites per area (1.478×10^{19} m^{-2}) and m_A denotes the molecular weight of adsorbent A. The desorption rate constant is again given by the equilibrium constant, i.e., equation 5.

In the presence of a solvent, the free energy of adsorption for A(g)+*→A* was calculated as,

$$\Delta G_{ads-solvent} = \Delta G_{ads-gas} + G_{A^*}(solv) - G_{Pd}(solv) \quad (7)$$

where $\Delta G_{ads-gas}$ is the free energy of adsorption under gas phase conditions and $G_{A^*}(solv)$ and $G_{Pd}(solv)$ are as before the solvation energies of the adsorbed molecule A and Pd surface immersed in the solvent, respectively. While it can be argued that the use of equation 6 is not

valid in liquid water, as long as there are no mass transfer limitations in the system and adsorption is not rate controlling (which is the case in most catalytic systems), adsorption is essentially an equilibrium process whose equilibrium constant is correctly described by our procedure. We also remark that the fugacity of species A in solution does not have to be calculated since it is at gas-liquid equilibrium equal to the partial pressure of species A in the gas phase which is assume to be ideal.

With the forward and reverse rate constants defined, rates of all elementary reactions can be expressed by mean-field rate laws. Considering that some of the adsorbed intermediates occupy multiple active sites (the number of occupied sites by each adsorbate is shown in Table 1), the rate expressions and steady state molecular balance equations are highly nonlinear. To solve the set of steady state differential reactor equations and to obtain the surface coverages of the intermediates, we used the BzzMath library[46] developed by Buzzi-Ferraris. No assumptions were made regarding rate-controlling steps.

3. Result and Discussion

3.1 Solvent effects on the adsorption strength of reaction intermediates

The investigated surface intermediates in the reaction network of the HDO of methyl propionate are listed in Table 1. The 41 intermediates can be classified into 7 different structural classes: (1) Methyl propionate and its hydrogenated derivatives, e.g. $CH_3CH_2COOCH_3$ and $CH_3CHCOOCH_3$, (2) propanoyl (CH_3CH_2CO) and its dehydrogenated derivatives such as CH_3CHCO etc. that are the reaction product of propanoyl-methoxy type dissociations ($CH_3CH_2CO—OCH_3$), (3) propionate (CH_3CH_2COO) and its dehydrogenated derivatives such as CH_3CHCOO etc., (4) methanol (CH_3OH) and its dehydrogenated derivatives such as methoxy

etc., (5) ethane (CH_3CH_3) and its dehydrogenated derivatives such as CH_3CH_2 etc. that are the products of a C-C bond cleavage in propanoyl (CH_3CH_2CO) type species, (6) methane (CH_4) and its dehydrogenated derivatives such as methyl (CH_3) etc. that are the products of propionate-methyl-type bond cleavages and $COOCH_3$ and $COOCH_2$ that are the products of the C-C bond cleavages in methyl propionate (CH_3CH_2—$COOCH_3$) and CH_3CH_2—$COOCH_2$ (the latter two groups do not participate in the dominant reaction mechanism since the C-C bond dissociation in methyl propionate, as well as the propionate-methyl bond dissociation are both thermodynamically and kinetically not favored). Finally, (7) there are small molecules or atoms such as, CO_2, CO, and H that need to be considered.

The presence of a solvent can modify the strength of adsorption of all classes of intermediates due to direct adsorbate-solvent interactions and indirect solvent-metal interactions that change the electronic structure of the metal and thus modify the metal-adsorbate interaction. To investigate the effects of the presence of liquid water and 1,4-dioxane on the adsorption strength of the intermediates involved in the HDO of methyl propionate, we computed the adsorption free energy in the absence and presence of solvents

$$A(g) + *\,(g) \leftrightarrow A^*(g) \qquad (8)$$

$$A(g) + *\,(l) \leftrightarrow A^*(l) \qquad (9)$$

and calculated the effects of the solvents on the free energy of adsorption of the surface intermediates as

$$\Delta\left(G_{ads,A}\right) = G_{ads,A}(l) - G_{ads,A}(g) = [G^{A*}(l) - G^{A*}(g)] - [G^*(l) - G^*(g)] \qquad (10)$$

where, $G_{ads,A}(l)$ and $G_{ads,A}(g)$ are the free energy of adsorption of a gas molecule of intermediate A in the presence and absence of solvent, $G^{A*}(l)$ and $G^{A*}(g)$ are the free energy of adsorbed A in the presence and absence of solvent, and $G^*(l)$ and $G^*(g)$ are the free energy of

the free active site/surface model of the catalyst in the presence and absence of solvent. We note that while many surface intermediates are unstable if separated from the Pd surface, the procedure described above permits understanding the effects of a solvent on the free energy of an adsorbed surface intermediate. Table 1 summarizes the calculated changes in the free energy of adsorption in the presence of water and 1,4-dioxane for all surface intermediates in the HDO of methyl propionate. Specifically, we observe that methyl propionate adsorbs stronger in the presence of water and 1,4-dioxane by 0.09 and 0.14 eV, respectively. Similarly, the adsorption strength of other dehydrogenated species is enhanced in the presence of the solvents. For example, in water, $CH_2CH_2COOCH_2$, $CH_3CHCOOCH_2$, and $CH_3CH_2COOCH_2$ adsorb stronger by 0.17, 0.13, and 0.12 eV, respectively. Likewise, in the presence of 1,4-dioxane adsorbed $CH_2CH_2COOCH_2$, $CH_2CHCOOCH_2$, and $CH_3CHCOOCH_3$ interact stronger with the Pd surface by 0.10, 0.09, and 0.06 eV, respectively.

Propanoyl and its dehydrogenated derivatives such as CH_3CHCO, CH_2CH_2CO are not affected by the presence of water and 1,4-dioxane. Similarly, non-polar hydrocarbons such as ethane, ethene, acethylene, methane, methyl and their dehydrogenated fragments are not affected by the presence of the solvents.

In contrast, propionate type species such as CH_3CHCOO and CH_3CCOO are the most affected species in water and 1,4-dioxane. Propionate (CH_3CH_2COO) itself is not significantly affected by solvents; however, CH_3CHCOO and CH_3CCOO adsorb stronger by 0.15 and 0.21 eV in water, and by 0.07 and 0.12 eV in 1,4-dioxane. These solvent effects can be understood by observing that propionate adsorbs via its two oxygen atoms, i.e., the oxygen atoms are not exposed to the liquid phase; while the dehydrogenated species CH_3CHCOO and CH_3CCOO adsorb strongly

through the unsaturated α-carbon, i.e., the 'locally charged' carboxyl group is exposed to the solvent molecules and stabilized by the solvent.

Propionate type intermediates eventually undergo C-C bond dissociations and form CO_2 and consequently, are important intermediates in the decarboxylation mechanism. Considering that these intermediates are stabilized significantly, an increase in activity of the decarboxylation mechanism can be expected.

Finally, CO adsorbs stronger in water by 0.08 eV and by 0.07 eV in 1,4-dioxane, while our model predicts that H atoms adsorb stronger by only 0.01 eV in both solvents. In this context, we note that Sha et al.[47] recently studied water solvent effects on various adsorbates and transition states in the oxygen reduction reaction over Pd(111) using their implicit solvation approach focusing on electrostatic interactions.[30] Overall, they observe larger solvent effects. However, considering that the COSMO-RS methodology applied here includes both electrostatic and temperature dependent non-bulk electrostatic contributions to the free energy such as first solvation shell effects in its parameterization, we continue to trust our solvent effects. Fortunately, both implicit solvent methodologies predict the same trends such that we expect our overall conclusions to be robust with regards to the uncertainties in the specific solvent effects of various adsorbates and transition states.

{Table 1 Here}

3.2 Solvent effects on various elementary reactions

In this section, we explain the effects of solvents on various elementary processes. Unbalanced solvation effects on the free energy of reactant, product, and transition states of an

elementary reaction can change the free energy of reaction (ΔG_{rxn}) and free energy of activation ($\Delta G^{\ddagger}$) of an elementary reaction step. The solvent effects on the free energy of activation and free energy of reaction for all elementary steps involved in the HDO of methyl propionate are summarized in Table 2 at a reaction temperature of 473 K.

{Table 2 Here}

We previously[6] studied the reaction network under gas-phase reaction conditions where we found that the rate controlling steps are dehydrogenation steps such as the dehydrogenation of α-, β-, and methoxy-end carbons in methyl propionate (steps 3, 4, and 5, respectively), as well as propanoyl-methoxy type dissociations such as step 2 ($CH_3CH_2COOCH_3$** + 2*↔ CH_3CH_2CO*** + CH_3O*) and step 12 ($CH_2CHCOOCH_3$*** + 1* ↔ CH_2CHCO*** +CH_3O*). Table 2 illustrates that the free energies of reaction and activation in the methyl propionate dehydrogenation steps (steps 3-5) are not significantly affected by the presence of water, since methyl propionate (reactant state), the dehydrogenated products, and the transition states for these steps are uniformly stabilized. In contrast, in 1,4-dioxane methyl propionate adsorbs stronger by 0.14 eV (Table 1), while the adsorption strength of the dehydrogenated intermediates such as $CH_3CHCOOCH_3$, $CH_2CH_2COOCH_3$, and $CH_3CH_2COOCH_2$ is only enhanced by 0.06, 0.06, and 0.05 eV, respectively, such that the reaction free energy of the dehydrogenation of the α-carbon (step 3) is increased by 0.07 eV and the activation barrier of this step is greater by 0.08 eV. Dehydrogenation of the β-carbon (step 4) in the presence of 1,4-dioxane is also less exothermic by 0.06 eV and possesses a higher barrier by 0.05 eV. Similarly,

the reaction free energy and activation barrier of the dehydrogenation of the methoxy-end carbon (step 5) is increased by 0.08 and 0.06 eV in 1,4-dioxane, respectively.

Propanoyl-methoxy type dissociations are also partially rate-controlling in the vapor phase and we showed above that methyl propionate and its derivative are stabilized in the presence of both water and 1,4-dioxane while propanoyl type intermediates are hardly affected by the presence of solvents. Additionally, the methoxy group is destabilized (adsorbs weaker on the Pd surface) in the presence of liquid water and 1,4-dioxane by 0.04 and 0.01 eV, respectively. In other words, the reactant states of propanoyl-methoxy type dissociations are stabilized while the product states are destabilized which leads to an increase in the reaction free energy of these reactions. For example, in water the endergonicity of step 2 ($CH_3CH_2COOCH_3$** + 2*↔ CH_3CH_2CO*** + CH_3O*) is increased by 0.17 eV (the free energy barrier is only increased by 0.01 eV). Similarly, in 1,4-dioxane this step has become more endergonic by 0.16 eV and the activation barrier is increased by 0.10 eV. Next, the free energy of reaction of step 12 ($CH_2CHCOOCH_3$*** + 1* ↔ CH_2CHCO*** +CH_3O*) is increased in water by 0.09 eV, while the reaction barrier is increased by 0.01 eV. In 1,4-dioxane, the reaction barrier is also increased by 0.01 eV, however, the reaction free energy is increased by only 0.04 eV because $CH_2CHCOOCH_3$ is less stabilized and the methoxy species of the product state is more stabilized in 1,4-dioxane than in water.

Overall, Table 2 shows that for all propanoyl-methoxy type dissociations, such as steps 2, 12, 17, and 21, the free energy of reaction is more affected by water than by 1,4-dioxane. This increase in endergonicity and also activation barrier of these rate-controlling dehydrogenation and propanoyl-methoxy type dissociation steps can potentially lower the overall activity of Pd. In contrast, the stronger adsorption of methyl propionate in water and 1,4-dioxane has the

potential to increase the activity. The net effect of these opposing solvent effects on the turnover frequency and reaction mechanism are discussed in more detail in section 3.3.

Finally, we observe that the dehydrogenation of propionate to CH_3CHCOO and eventually CH_3CCOO (step 61 and step 63) are facilitated significantly in both water and 1,4-dioxane. For example, the activation barrier of step 61 is decreased by 0.24 eV in water (the reaction free energy is decreased by 0.17 eV). These steps play an important role in the decarboxylation mechanism, as propionate and its dehydrogenated derivatives can undergo a C-C bond cleavage to form CO_2. However, our previous gas phase results suggested that the decarboxylation mechanism is not the dominant mechanism and consequently, only microkinetic modeling can determine if these relatively large solvent effects have any significant effect on the observed kinetics and reaction mechanism.

3.3 Mean-field microkinetic modeling

We previously developed a mean-field microkinetic model for the reaction mechanism of the HDO of methyl propionate over a Pd (111) surface model under gas-phase conditions.[6] In this study, we extended our previous model by the presence of a liquid phase of 1,4-dioxane and water. Otherwise, the reaction conditions are equivalent in both studies. All calculations were carried out at a temperature of 473 K and partial pressures of propionic acid and H_2 of 0.01 and 0.2 bar, respectively.[48] The partial pressures of CO_2 and CO were set to 0.001 bar which corresponds to approximately 10% conversion. It is noted that our results and conclusions seem to be insensitive to the reaction conditions. Next, we note that a method similar to Grabow *et al.*[49] was used for determining coverage dependent adsorption energies of CO, H, and CH_3C.

More details about the lateral interactions used in the microkinetic model for this study can be found in the supporting information of our previously published paper.

To facilitate the discussion of solvent effects, we briefly recap our gas phase results. In the absence of a solvent, the most abundant surface intermediates were adsorbed hydrogen, CO, and CH_3C with surface coverages of 67%, 20%, and 7%, respectively (the free site coverage is 6%). The overall turnover frequency (TOF) was calculated to be 3.42×10^{-7} s^{-1}, which is quite small but typical for computational studies of flat metal surfaces. Decarbonylation was identified to be the dominant mechanism (dominant pathway: $CH_3CH_2COOCH_3$→ $CH_3CHCOOCH_3$→$CH_2CHCOOCH_3$→$CH_2CHCO+OCH_3$→…→$CH_3CH_3+CO+CH_3OH$) and the TOF of the decarboxylation pathways were predicted to be at least 3 orders of magnitude smaller than the TOF of the decarbonylation pathways. A schematic of our previous result is shown in Figure 1 and the TOFs of all elementary steps in the presence and absence of solvents is given in Table 3. Calculated rate constants and turnover frequency of all elementary steps in the HDO of methyl propionate over Pd (111) (in the absence and presence of solvents) are presented in Table 3 and 4.

Liquid water effects

The overall turnover frequency was calculated to be 1.64×10^{-8} s^{-1} which is an order of magnitude smaller than the gas-phase TOF (3.42×10^{-7} s^{-1}). In the most dominant pathway methyl propionate goes through dehydrogenation of the α- and β-carbon to form $CH_2CHCOOCH_3$. $CH_2CHOOCH_3$ goes through C-O bond dissociation to form CH_2CHO and methoxy (CH_3O). Next, methoxy gets hydrogenated to methanol and CH_2CHO goes through hydrogenation and finally C-C cleavage to form C_2 hydrocarbons and CO ($CH_3CH_2COOCH_3$→

$CH_3CHCOOCH_3 \rightarrow CH_2CHCOOCH_3 \rightarrow CH_2CHCO+OCH_3 \rightarrow \ldots \rightarrow CH_3CH_3+CO+CH_3OH$). This pathway is identical to the dominant pathway in the absence of water. A schematic of the TOFs of the most important reaction pathways in the presence of liquid water is shown in Figure 1. The most abundant surface intermediates were hydrogen, CO, and CH_3C with surface coverages of 69.8%, 18.6%, and 9.9%, respectively. The decrease in the rate of the reaction in the presence of water can be explained by both a decrease in the availability of free sites (1.7%) and an inhibition of some of the rate-controlling steps by water. To explain the changes in the surface coverages of the dominant surface species (the H coverage increased by 3%, the CO coverage decreased by 1% and the CH_3C coverage increased by 3%), it is necessary to consider both the direct effect of solvents in stabilizing the surface species and the indirect effect of lateral surface interactions and solvents modifying the rate of removal of the surface intermediates. For example, the adsorption strength of a hydrogen and CH_3C is hardly affected by the presence of water while adsorbed CO is stabilized by 0.08 eV (see Table 1). However, water inhibits the removal of CH_3C from the surface (steps 50, 51, and 53), thus, increasing its surface coverage. Next, our previous adsorption energy analysis for coverage dependent intermediates shows that there are attractive interactions between CH_3C and H while there are repulsive interactions between CH_3C and CO.[6] In other words, the attractive interactions between H and CH_3C increase the H coverage in the presence of a larger amount of CH_3C, while the repulsive interactions slightly decrease the CO coverage despite the solvent stabilization of the adsorbed CO molecule. Overall, the free site coverage decreases due to the presence of water.

Finally, the decarbonylation mechanism remains the dominant mechanism in liquid water. In the absence of a solvent, the ratio of the TOF of the dominant decarboxylation pathway ($CH_3CH_2COOCH_3 \rightarrow CH_3CH_2COOCH_2 \rightarrow CH_3CH_2COO+CH_2 \rightarrow \ldots \rightarrow CH_3CH_3+CO_2+$

CH_4) to the overall TOF was 0.001 (0.1%). As expected, the importance of the decarboxylation pathway increases to 1.3% (of the total TOF) due to a more facile dehydrogenation of propionate and its derivative, however, the TOF of the decarbonylation pathways remain 2 orders of magnitude higher than the decarboxylation pathways.

{Figure 1 here}

Liquid 1,4-dioxane effects

The overall turnover frequency of the HDO of methyl propionate over Pd (111) in the presence of 1,4-dioxane was calculated to be 2.86×10^{-7} s^{-1}. The most abundant surface intermediates were again hydrogen, CO, CH_3C, and free sites with surface coverages of 66%, 21%, 8%, and 4%, respectively. Turnover frequency and surface coverages are very similar to the gas phase results, i.e., the TOF is one order of magnitude larger in 1,4-dioxane than in liquid water. A schematic of the TOFs of the most important reaction mechanism in the presence of 1,4-dioxane is shown in Figure 2. The dominant reaction mechanism is the same as in the vapor and liquid water phase ($CH_3CH_2COOCH_3 \rightarrow CH_3CHCOOCH_3 \rightarrow CH_2CHCOOCH_3 \rightarrow CH_2CHCO+OCH_3 \rightarrow \ldots \rightarrow CH_3CH_3+CO+CH_3OH$). Finally, the dehydrogenation steps of propionate or CH_3CHCOO (steps 61and 63) are less facilitated in 1,4-dioxane than in water such that the decarboxylation pathways only contribute 0.4% to the overall TOF which is slightly larger than in the gas phase (0.1%) but significantly lower than in liquid water (1.3%).

{Figure 2 here}

{Table 3 and 4 here}

3.4 Apparent activation barrier, reaction orders, and sensitivity analysis

Vapor phase

In the absence of solvents, the apparent activation barrier, reaction orders, and a sensitivity analysis of the HDO of methyl propionate over Pd (111) have been thoroughly discussed in our previous work.[3] In order to better understand the effects of solvents on these parameters, we briefly review the vapor-phase data. The apparent activation barrier was computed in the temperature range of 423 to 523 K.

$$E_a = RT^2\left(\frac{\partial \ln(r)}{\partial T}\right)_{p_i} \tag{11}$$

Our vapor phase model predicts an apparent activation energy of 1.01 eV. The reaction order with respect to hydrogen was calculated at 473 K in the range of 0.05 to 0.4 bar. Similarly, the reaction order of methyl propionate and CO were calculated at 473 K and a pressure range of 0.005 to 0.1 bar and 0.0001 to 0.1 bar, respectively.

$$\alpha_i = \left(\frac{\partial \ln(r)}{\partial \ln(p_i)}\right)_{T,p_{j\neq i}} \tag{12}$$

The reaction order with respect to methyl propionate was calculated to be +1.0, which can be explained by the small methyl propionate coverage in our model. The reaction order with respect to CO is -0.49. Finally, the reaction order of H_2 is -0.07, which indicates that under the investigated reaction conditions the hydrogen coverage is balanced with the free site coverage

such that the dehydrogenation rates prior to decarbonylation are balanced with the hydrogenation processes required for desorption of the reaction products.

To understand the sensitivity of our model on its parameters (free energies of various states) and to determine the rate controlling steps and intermediates in the mechanism, we computed Campbell's degrees of rate and thermodynamic control,[50-53] X_{RC} and X_{TRC}.

$$X_{\mathrm{RC},i} = \frac{k_i}{r}\left(\frac{\partial r}{\partial k_i}\right)_{K_i, k_j \neq k_i} \quad , \quad X_{\mathrm{TRC},n} = \frac{1}{r}\left(\frac{\partial r}{\partial\left(\frac{-G_n^0}{RT}\right)}\right)_{G_{m\neq n}^0, G_i^{0,\mathrm{TS}}} \tag{13}$$

where r is the overall rate of reaction, k_i is the forward rate constant for step i, K_i equilibrium constant for step i, R is the ideal gas constant, T denotes the reaction temperature, and G_n^0 is the free energy of adsorbate n. We note that that the degree of rate control for a single rate-controlling step in a reaction mechanism is one; and for transition and intermediate states that do not influence the overall activity, the degrees of thermodynamic and rate control are zero. The most rate controlling steps are propanoyl-methoxy type bond dissociations and dehydrogenations of α-, β-, and methoxy-end carbons of methyl propionate. Reaction step 2 ($CH_3CH_2COOCH_3$** + 2*↔ CH_3CH_2CO*** + CH_3O*), a propanoyl-methoxy dissociation, is the most rate-controlling C-O bond dissociation step with an X_{RC} of 0.17. Additionally, step 12 ($CH_2CHCOOCH_3$*** + 1* ↔ CH_2CHCO*** +CH_3O*) and step 28 ($CH_3CH_2COOCH_2$*** + 3* ↔ CH_3CH_2CO*** + OCH_2***) are also rate-controlling with an X_{RC} of 0.09 and 0.02, respectively, such that the sum of the C-O bond dissociation rate control values is 0.28.

Next, dehydrogenation of the α-carbon of methyl propionate (step 2) is the most rate-controlling dehydrogenation step with an X_{RC} of 0.35. Dehydrogenation of the methoxy-end carbon of methyl propionate (step 5) has an X_{RC} of 0.19, dehydrogenation of the β-carbon of

methyl propionate (step 4) has an X_{RC} of 0.05, and finally dehydrogenation of the β-carbon of $CH_3CHCOOCH_3$*** (step 8: $CH_3CHCOOCH_3$*** + 1* ↔ $CH_2CHCOOCH_3$*** + H*) has an X_{RC} of 0.03.

Liquid water

In the presence of liquid water, our model predicts an apparent activation energy of 2.40 eV for the HDO of methyl propionate over Pd (111) which is significantly larger than in the absence of water (1.01 eV). The apparent activation barrier is higher than the activation barrier of the rate-controlling steps which are in the range of 0.8 to 0.9 eV. This can be explained with a crowded surface that becomes less crowded at higher temperatures, leading to a significant increase in the reaction rate. Considering that in the presence of water, the surface is crowded by hydrogen and CH_3C, the apparent activation energy is significantly higher than under vapor-phase condition. Next, our liquid water model predicts a reaction order of +1.0 with respect to methyl propionate similar to our vapor phase model. This can be explained by the endergonicity of the adsorption of methyl propionate, $\Delta G_{ads\text{-}water}$= 0.36, and its low coverage on Pd. The reaction order with respect to CO was calculated to be -0.19 which is lower than in the vapor phase model (-0.49) which suggests a reduced CO poisoning in liquid water due to a slightly reduced CO coverage. Unfortunately, we were not able to compute a reliable hydrogen reaction order due to significant numerical noise in our liquid water model at very small TOF values (~10^{-20}- 10^{-8} s^{-1}) at a larger hydrogen pressure. However, we expect that the reaction order of hydrogen in water is significantly more negative than in the gas-phase (-0.07) since the coverage of hydrogen increased in some of our simulations to over 70% leading to significant hydrogen poisoning.

The rate controlling steps in the presence of water are still dehydrogenation steps as well as propanoyl-methoxy type dissociations. However, the values of the degree of rate control of these steps, which indicates the importance of a step in the overall kinetics, were altered in water. In the following, we list the vapor phase value in [ ] next to the liquid water values. The rate-controlling dehydrogenation steps in water are step 3 ($CH_3CH_2COOCH_3$** + 2* ↔ $CH_3CHCOOCH_3$*** + H*) with X_{RC} of 0.14 [0.35], step 4 ($CH_3CH_2COOCH_3$** + 2* ↔ $CH_2CH_2COOCH_3$*** + H*) with X_{RC} of 0.04 [0.05], and step 5 ($CH_3CH_2COOCH_3$** + 2* ↔ $CH_3CH_2COOCH_2$*** + H*) with X_{RC} of 0.07 [0.19]. Overall, the presence of water decreased significantly the importance of the dehydrogenation steps on the kinetics of the HDO of methyl propionate. This observation can be explained by the fact that propanoyl-methoxy type dissociations are inhibited in water, and the activity of methyl propionate in water is more limited by the activation of propanoyl-methoxy type C-O bond dissociations than dehydrogenation steps. The degree of rate control analysis also confirms that propanoyl-methoxy type dissociations are more influential in liquid water. Step 2 ($CH_3CH_2COOCH_3$** + 2*↔ CH_3CH_2CO*** + CH_3O*) has an X_{RC} of 0.21 [0.17]. The X_{RC} of step 12 ($CH_2CHCOOCH_3$*** + 1* ↔ CH_2CHCO*** +CH_3O*) was calculated to be 0.23 [0.09], and finally step 28 ($CH_3CH_2COOCH_2$*** + 3* ↔ CH_3CH_2CO*** + OCH_2***) has an X_{RC} of 0.13 [0.02].

Finally, the degree of thermodynamic rate control for CO was calculated to be -0.20 [-0.57] which indicates again that CO poisoning is less important in liquid water. The degree of thermodynamic rate control for H could again not be computed due to numerical inaccuracies; however, we expect a significant negative thermodynamic rate control due to a high H coverage on the surface.

Liquid 1,4-dioxane

Pd (111) in liquid 1,4-dioxane displays a very similar activity to Pd (111) under gas-phase conditions. In 1,4-dioxane, dehydrogenation steps are inhibited (see Table 2) while propanoyl-methoxy type dissociations are not as significant as in water. Consequently, the overall kinetics is primarily limited by dehydrogenation steps. For example, step 3 ($CH_3CH_2COOCH_3$** + 2* ↔ $CH_3CHCOOCH_3$*** + H*), step 4 ($CH_3CH_2COOCH_3$** + 2* ↔ $CH_2CH_2COOCH_3$*** + H*), and step5 ($CH_3CH_2COOCH_3$** + 2* ↔ $CH_3CH_2COOCH_2$*** + H*) have X_{RC} values of 0.29 [0.34], 0.07 [0.05], and 0.18 [0.19] respectively (the numbers in [ ] are again the X_{RC} values in the absence of solvent). In addition, propanoyl-methoxy type dissociations such as step 2 ($CH_3CH_2COOCH_3$** + 2*↔ CH_3CH_2CO*** + CH_3O*), step 12 ($CH_2CHCOOCH_3$*** + 1* ↔ CH_2CHCO*** +CH_3O*), and step 28 ($CH_3CH_2COOCH_2$*** + 3* ↔ CH_3CH_2CO*** + OCH_2***) have significant X_{RC} of 0.10 [0.17], 0.09 [0.12], and 0.04 [0.02], respectively, that are however significantly lower than in liquid water.

Similar to vapor-phase results, the reaction order with respect to methyl propionate, CO and hydrogen was calculated to be +1.0, -0.48, and -0.11, respectively. Only the apparent activation energy of 1.49 eV was found to be larger in the presence of 1,4-dioxane than in the vapor phase which can again be explained by an increased surface coverage in the presence of solvents.

Finally, the X_{TRC} values of CO and H show a similar trend to the gas-phase results where CO possesses an X_{TRC} of -0.75 and the X_{TRC} of H is -0.05. We note that while the trend of the thermodynamic degrees of rate-control in1,4-dioxane is very similar to the gas-phase results, it is

quite different to the liquid water results, where adsorbed H plays a more important role in the activity and the CO adsorption strength is of lesser importance.

4. Conclusions

The effects of liquid water and 1,4-dioxane were investigated on the hydrodeoxygenation of methyl propionate over a Pd (111) surface model. Using an implicit solvation scheme and microkinetic reaction models in various reaction environments, we studied the effects of the solvents on the adsorption strength of various surface intermediates, the reaction rate parameters of various elementary reaction steps, and the overall effect of solvents on the reaction mechanism and kinetic parameters. The overall activity of Pd (111) in liquid water was lower than in 1,4-dioxane which is very similar to the activity in the vapor phase. The decarbonylation mechanism was identified to be the most dominant mechanism in all reaction media; however, in the presence of water, propionate and its hydrogenated derivatives—that are key intermediates in the decarboxylation mechanism—are stabilized such that the decarboxylation mechanism is facilitated but still only contributes about 1.3% to the total rate. H, CO, and CH_3C are the most abundant surface intermediates in all reaction environments. In water, the coverage of hydrogen is increased which results in a decrease in the free site coverage and consequently a lower turnover frequency. In both the presence and absence of solvents, dehydrogenation steps as well as propanoyl-methoxy type dissociations were identified to be the rate controlling steps. In water, propanoyl-methoxy type dissociations become more endergonic and their activation barriers increase such that the overall activity becomes more limited by these propanoyl-methoxy type dissociations, i.e., the importance of the dehydrogenation steps is diminished. In contrast, in 1,4-dioxane and in the vapor phase dehydrogenation steps are most rate controlling and

propanoyl-methoxy type dissociations are of lesser importance. Overall, the nonpolar, aprotic solvent 1,4-dioxane has only a minor effect on the activity and reaction mechanism of the HDO of methyl propionate over Pd (111); in contrast, the activity of Pd (111) is significantly affected by liquid water in ways often difficult to predict without detailed analysis.

5. Acknowledgement

This work has been supported by the National Science Foundation under Grant No. CBET-1159863 and in part by the U.S. Department of Energy, Office of Basic Energy Sciences, Chemical Sciences Division under Contract DE-FG02-11ER16268 (DE-SC0007167) and the USC future fuels program and USC NanoCenter. This research used resources of the National Energy Research Scientific Computing Center, a DOE Office of Science User Facility supported by the Office of Science of the U.S. Department of Energy under Contract No. DE-AC02-05CH11231 and in part by XSEDE resources provided by the National Institute for Computational Sciences (NICS), Texas advanced Computing Center (TACC), and Purdue University under grant number TG-CTS090100. Finally, computing resources from the USC NanoCenter and USC's High Performance Computing Group are gratefully acknowledged.

Appendix A. Supplementary material

Supplementary data associated with this article can be found, in the online version, at http://dx.doi.org/XXX.

References

1. Huber, G. W.; O'Connor, P.; Corma, A., Processing Biomass in Conventional Oil Refineries: Production of High Quality Diesel by Hydrotreating Vegetable Oils in Heavy Vacuum Oil Mixtures. *Appl. Catal. A* **2007**, *329*, 120-129.
2. Donnis, B.; Egeberg, R. G.; Blom, P.; Knudsen, K. G., Hydroprocessing of Bio-Oils and Oxygenates to Hydrocarbons. Understanding the Reaction Routes. *Topics Catal.* **2009**, *52*, 229-240.
3. Kubicka, D.; Simacek, P.; Zilkova, N., Transformation of Vegetable Oils into Hydrocarbons over Mesoporous-Alumina-Supported Como Catalysts. *Topics Catal.* **2009**, *52*, 161-168.
4. Lu, J. M.; Behtash, S.; Faheem, M.; Heyden, A., Microkinetic Modeling of the Decarboxylation and Decarbonylation of Propanoic Acid over Pd(111) Model Surfaces Based on Parameters Obtained from First Principles. *J. Catal.* **2013**, *305*, 56-66.
5. Lu, J. M.; Behtash, S.; Heyden, A., Theoretical Investigation of the Reaction Mechanism of the Decarboxylation and Decarbonylation of Propanoic Acid on Pd(111) Model Surfaces. *Journal of Physical Chemistry C* **2012**, *116*, 14328-14341.
6. Behtash, S.; Lu, J.; Heyden, A., Theoretical Investigation of the Hydrodeoxygenation of Methyl Propionate over Pd (111) Model Surfaces. *Catalysis Science & Technology* **2014**, *4*, 3981.
7. Blaser, H. U.; Jalett, H. P.; Wiehl, J., Enantioselective Hydrogenation of Alpha-Ketoesters with Cinchona-Modified Platinum Catalysts - Effect of Acidic and Basic Solvents and Additives. *Journal of Molecular Catalysis* **1991**, *68*, 215-222.
8. Wehrli, J. T.; Baiker, A.; Monti, D. M.; Blaser, H. U.; Jalett, H. P., Enantioselective Hydrogenation of Alpha-Ketoesters - Influence of Reaction Medium and Conversion. *Journal of Molecular Catalysis* **1989**, *57*, 245-257.
9. Gilbert, L.; Mercier, C., Solvent Effects in Heterogeneous Catalysis - Application to the Synthesis of Fine Chemicals. *Heterogeneous Catalysis and Fine Chemicals Iii* **1993**, *78*, 51-66.
10. Singh, U. K.; Vannice, M. A., Kinetics of Liquid-Phase Hydrogenation Reactions over Supported Metal Catalysts - a Review. *Applied Catalysis a-General* **2001**, *213*, 1-24.
11. Koopman, P. G. J.; Buurmans, H. M. A.; Kieboom, A. P. G.; Vanbekkum, H., Solvent-Reactant-Support Interactions in Liquid-Phase Hydrogenation. *Recueil Des Travaux Chimiques Des Pays-Bas-Journal of the Royal Netherlands Chemical Society* **1981**, *100*, 156-161.
12. Wauquier, J. P.; Jungers, J. C., La Cinetique Quantitative En Catalyse Heterogene - Linfluence Du Milieu Sur Lactivite Et La Selectivite Du Catalyseur. *Bulletin De La Societe Chimique De France* **1957**, 1280-1288.
13. Cerveny, L.; Kuncova, M.; Ruzicka, V., Effect of Composition of the Solvent on the Selectivity of Competitive Hydrogenation of 2-Methyl-3-Butene-2-Ol and 1-Hexene. *Reaction Kinetics and Catalysis Letters* **1982**, *19*, 219-222.
14. Rajadhyaksha, R. A.; Karwa, S. L., Solvent Effects in Catalytic-Hydrogenation. *Chemical Engineering Science* **1986**, *41*, 1765-1770.
15. Mathew, K.; Sundararaman, R.; Letchworth-Weaver, K.; Arias, T. A.; Hennig, R. G., Implicit Solvation Model for Density-Functional Study of Nanocrystal Surfaces and Reaction Pathways. *The Journal of Chemical Physics* **2014**, *140*, 084106.
16. Faheem, M.; Suthirakun, S.; Heyden, A., New Implicit Solvation Scheme for Solid Surfaces. *J. Phys. Chem. C* **2012**, *116*, 22458-22462.
17. Zope, B. N.; Hibbitts, D. D.; Neurock, M.; Davis, R. J., Reactivity of the Gold/Water Interface During Selective Oxidation Catalysis. *Science* **2010**, *330*, 74-78.
18. Jacob, T.; Goddard, W. A., Water Formation on Pt and Pt-Based Alloys: A Theoretical Description of a Catalytic Reaction. *ChemPhysChem* **2006**, *7*, 992-1005.

19. Wang, H.-F.; Liu, Z.-P., Formic Acid Oxidation at Pt/H2o Interface from Periodic Dft Calculations Integrated with a Continuum Solvation Model. *The Journal of Physical Chemistry C* **2009**, *113*, 17502-17508.
20. Michel, C.; Zaffran, J.; Ruppert, A. M.; Matras-Michalska, J.; Jedrzejczyk, M.; Grams, J.; Sautet, P., Role of Water in Metal Catalyst Performance for Ketone Hydrogenation: A Joint Experimental and Theoretical Study on Levulinic Acid Conversion into Gamma-Valerolactone. *Chemical Communications* **2014**, *50*, 12450-12453.
21. Faheem, M.; Heyden, A., Hybrid Quantum Mechanics/Molecular Mechanics Solvation Scheme for Computing Free Energies of Reactions at Metal–Water Interfaces. *Journal of Chemical Theory and Computation* **2014**, *10*, 3354-3368.
22. Behtash, S.; Lu, J. M.; Faheem, M.; Heyden, A., Solvent Effects on the Hydrodeoxygenation of Propanoic Acid over Pd(111) Model Surfaces (Vol 16, Pg 605, 2014). *Green Chemistry* **2014**, *16*, 4427-4428.
23. Behtash, S.; Lu, J. M.; Faheem, M.; Heyden, A., Solvent Effects on the Hydrodeoxygenation of Propanoic Acid over Pd(111) Model Surfaces. *Green Chemistry* **2014**, *16*, 605-616.
24. Lugo-José, Y. K.; Behtash, S.; Nicholson, M.; Monnier, J. R.; Heyden, A.; Williams, C. T., Unraveling the Mechanism of Propanoic Acid Hydrodeoxygenation on Palladium Using Deuterium Kinetic Isotope Effects. *Journal of Molecular Catalysis A: Chemical* **2015**, *406*, 85-93.
25. Behtash, S.; Lu, J.; Williams, C. T.; Monnier, J. R.; Heyden, A., Effect of Palladium Surface Structure on the Hydrodeoxygenation of Propanoic Acid: Identification of Active Sites. *The Journal of Physical Chemistry C* **2015**, *119*, 1928-1942.
26. Lugo-Jose, Y. K.; Monnier, J. R.; Heyden, A.; Williams, C. T., Hydrodeoxygenation of Propanoic Acid over Silica-Supported Palladium: Effect of Metal Particle Size. *Catalysis Science & Technology* **2014**, *4*, 3909-3916.
27. Medford, A. J.; Wellendorff, J.; Vojvodic, A.; Studt, F.; Abild-Pedersen, F.; Jacobsen, K. W.; Bligaard, T.; Nørskov, J. K., Assessing the Reliability of Calculated Catalytic Ammonia Synthesis Rates. *Science* **2014**, *345*, 197-200.
28. Marenich, A. V.; Ding, W.; Cramer, C. J.; Truhlar, D. G., Resolution of a Challenge for Solvation Modeling: Calculation of Dicarboxylic Acid Dissociation Constants Using Mixed Discrete–Continuum Solvation Models. *The Journal of Physical Chemistry Letters* **2012**, *3*, 1437-1442.
29. Chung, L. W., et al., The Oniom Method and Its Applications. *Chemical Reviews* **2015**, *115*, 5678-5796.
30. Sha, Y.; Yu, T. H.; Liu, Y.; Merinov, B. V.; Goddard, W. A., Theoretical Study of Solvent Effects on the Platinum-Catalyzed Oxygen Reduction Reaction. *Journal of Physical Chemistry Letters* **2010**, *1*, 856-861.
31. Klamt, A., Conductor-Like Screening Model for Real Solvents - a New Approach to the Quantitative Calculation of Solvation Phenomena. *Journal of Physical Chemistry* **1995**, *99*, 2224-2235.
32. Klamt, A.; Jonas, V.; Burger, T.; Lohrenz, J. C. W., Refinement and Parametrization of Cosmo-Rs. *J. Phys. Chem. A* **1998**, *102*, 5074-5085.
33. Klamt, A., *Cosmo-Rs: From Quantum Chemistry to Fluid Phasethermodynamics and Drug Design*; Elsevier Science, 2005.
34. Ahlrichs, R.; Bar, M.; Haser, M.; Horn, H.; Kolmel, C., Electronic-Structure Calculations on Workstation Computers - the Program System Turbomole. *Chem. Phys. Lett.* **1989**, *162*, 165-169.
35. Treutler, O.; Ahlrichs, R., Efficient Molecular Numerical-Integration Schemes. *Journal of Chemical Physics* **1995**, *102*, 346-354.
36. Kerdcharoen, T.; Rode, B. M., What Is the Solvation Number of Na^+ in Ammonia? An Ab Initio Qm/Mm Molecular Dynamics Study. *J. Phys. Chem. A* **2000**, *104*, 7073-7078.

37. Kresse, G.; Hafner, J., Abinitio Molecular-Dynamics for Liquid-Metals. *Physical Review B* **1993**, *47*, 558-561.
38. Kresse, G.; Furthmuller, J., Efficiency of Ab-Initio Total Energy Calculations for Metals and Semiconductors Using a Plane-Wave Basis Set. *Comput. Mater. Sci.* **1996**, *6*, 15-50.
39. Wicke, E.; Brodowsky, H.; Zuchner, H., Hydrogen in Palladium and Palladium Alloys. *Topics in Applied Physics* **1978**, *29*, 73-155.
40. Weigend, F.; Haser, M.; Patzelt, H.; Ahlrichs, R., Ri-Mp2: Optimized Auxiliary Basis Sets and Demonstration of Efficiency. *Chemical Physics Letters* **1998**, *294*, 143-152.
41. Weigend, F.; Ahlrichs, R., Balanced Basis Sets of Split Valence, Triple Zeta Valence and Quadruple Zeta Valence Quality for H to Rn: Design and Assessment of Accuracy. *Physical Chemistry Chemical Physics* **2005**, *7*, 3297-3305.
42. Weigend, F., Accurate Coulomb-Fitting Basis Sets for H to Rn. *Physical Chemistry Chemical Physics* **2006**, *8*, 1057-1065.
43. Eichkorn, K.; Treutler, O.; Ohm, H.; Haser, M.; Ahlrichs, R., Auxiliary Basis-Sets to Approximate Coulomb Potentials (Vol 240, Pg 283, 1995). *Chemical Physics Letters* **1995**, *242*, 652-660.
44. Eichkorn, K.; Weigend, F.; Treutler, O.; Ahlrichs, R., Auxiliary Basis Sets for Main Row Atoms and Transition Metals and Their Use to Approximate Coulomb Potentials. *Theoretical Chemistry Accounts* **1997**, *97*, 119-124.
45. Von Arnim, M.; Ahlrichs, R., Performance of Parallel Turbomole for Density Functional Calculations. *Journal of Computational Chemistry* **1998**, *19*, 1746-1757.
46. Buzzi-Ferraris, G., *"BzzMath: Numerical libraries in C++", Politecnico di Milano: www.chem.polimi.it/homes/gbuzzi*.
47. Sha, Y.; Yu, T. H.; Merinov, B. V.; Goddard, W. A., Dft Prediction of Oxygen Reduction Reaction on Palladium-Copper Alloy Surfaces. *Acs Catalysis* **2014**, *4*, 1189-1197.
48. Lugo-Jose, Y. K.; Monnier, J. R.; Williams, C. T., Gas-Phase, Catalytic Hydrodeoxygenation of Propanoic Acid, over Supported Group Viii Noble Metals: Metal and Support Effects. *Appl. Catal. A* **2014**, *469*, 410-418.
49. Grabow, L. C.; Hvolbaek, B.; Norskov, J. K., Understanding Trends in Catalytic Activity: The Effect of Adsorbate-Adsorbate Interactions for Co Oxidation over Transition Metals. *Topics Catal.* **2010**, *53*, 298-310.
50. Campbell, C. T., Micro- and Macro-Kinetics: Their Relationship in Heterogeneous Catalysis. *Topics in Catalysis* **1994**, *1*, 353-366.
51. Campbell, C. T., Finding the Rate-Determining Step in a Mechanism - Comparing Dedonder Relations with the "Degree of Rate Control". *Journal of Catalysis* **2001**, *204*, 520-524.
52. Stegelmann, C.; Andreasen, A.; Campbell, C. T., Degree of Rate Control: How Much the Energies of Intermediates and Transition States Control Rates. *Journal of the American Chemical Society* **2009**, *131*, 8077-8082.
53. Kozuch, S.; Shaik, S., A Combined Kinetic-Quantum Mechanical Model for Assessment of Catalytic Cycles: Application to Cross-Coupling and Heck Reactions. *Journal of the American Chemical Society* **2006**, *128*, 3355-3365.

Table 1. Effect of solvents on adsorption strength of intermediates in the HDO of methyl propionate over Pd(111) model surfaces at a temperature of 473 K. Δ(ΔG) is the difference in the adsorption free energy of intermediate A, in the presence ($A(g) + * (l) \leftrightarrow A^*(l)$) and absence of solvents ($A(g) + * (g) \leftrightarrow A^*(g)$). Asterisk (*) represents a surface adsorption site and number of required active sites are indicated by multiple asterisks.

Reaction	Water	1,4-Dioxane
	Δ(ΔG) / eV	Δ(ΔG) / in eV
$CH_3CH_2COOCH_3$**	-0.09	-0.14
$CH_3CHCOOCH_3$***	-0.08	-0.06
$CH_3CH_2COOCH_2$***	-0.12	-0.05
$CH_2CH_2COOCH_3$***	-0.09	-0.06
$CH_2CHCOOCH_3$***	-0.09	-0.05
$CH_3CHCOOCH_2$***	-0.13	-0.06
$CH_2CH_2COOCH_2$***	-0.17	-0.10
$CH_2CHCOOCH_2$****	-0.17	-0.09
$CHCHCOOCH_3$****	-0.11	-0.06
CH_3CH_2CO***	0.04	0.00
CH_3CHCO***	-0.01	-0.01
CH_2CH_2CO***	0.00	0.00
CH_3CCO***	-0.02	-0.02
CH_2CHCO***	-0.03	-0.02
CHCHCO****	-0.04	-0.01
CH_3CH_2COO**	0.01	-0.03
CH_3CHCOO***	-0.15	-0.07
CH_3CCOO***	-0.21	-0.12
CH_3OH*	-0.07	-0.06
CH_3O*	0.04	0.01
CH_2O***	-0.03	-0.02
CHO***	0.01	0.01
$COOCH_3$***	-0.05	-0.03
$COOCH_2$****	-0.02	-0.02
CH_3CH_3*	0.03	0.00
CH_3CH_2*	0.03	0.01
CH_3CH**	0.00	0.00
CH_2CH_2**	0.02	0.01
CH_2CH***	0.00	0.00
CH_3C***	0.00	-0.01
CH_2C**	-0.02	-0.01
CHCH***	-0.02	0.00
CH_4*	0.04	0.02
CH_3*	0.03	0.02
CH_2**	0.02	0.02

CO*	-0.08	-0.07
CO_2*	0.02	0.00
H*	-0.01	-0.01
OH*	-0.05	-0.03
H_2O*	-0.12	-0.07

Table 2. Reaction free energies in eV for all elementary reaction steps in the hydrodeoxygenation of methyl propionate over a Pd(111) model surface at a temperature of 473 K in the vapor phase and in the presence of liquid water and 1,4-dioxane solvents.

	Reaction	Gas		Water		1,4-Dioxane	
		ΔG_{rxn}	$\Delta G^{\ddagger}$	ΔG_{rxn}	$\Delta G^{\ddagger}$	ΔG_{rxn}	$\Delta G^{\ddagger}$
1	$CH_3CH_2COOCH_3$** + 1* ↔ CH_3CH_2COO** + CH_3*	-0.47	1.57	-0.35	1.55	-0.35	1.61
2	$CH_3CH_2COOCH_3$** + 2*↔ CH_3CH_2CO*** + CH_3O*	0.20	0.79	0.37	0.80	0.35	0.89
3	$CH_3CH_2COOCH_3$** + 2* ↔ $CH_3CHCOOCH_3$*** + H*	-0.02	0.74	-0.02	0.74	0.05	0.82
4	$CH_3CH_2COOCH_3$** + 2* ↔ $CH_2CH_2COOCH_3$*** + H*	0.16	0.84	0.14	0.80	0.22	0.89
5	$CH_3CH_2COOCH_3$** + 2* ↔ $CH_3CH_2COOCH_2$*** + H*	0.09	0.78	0.05	0.75	0.17	0.84
6	$CH_3CHCOOCH_3$*** + 1* ↔ CH_3CHCOO*** + CH_3*	-0.04	1.63	-0.08	1.58	-0.03	1.61
7	$CH_3CHCOOCH_3$*** + 1* ↔ CH_3CHCO*** + CH_3O*	0.24	0.74	0.35	0.80	0.30	0.78
8	$CH_3CHCOOCH_3$*** + 1* ↔ $CH_2CHCOOCH_3$*** + H*	-0.43	0.50	-0.46	0.46	-0.44	0.49
9	$CH_3CHCOOCH_3$*** + 1* ↔ $CH_3CHCOOCH_2$*** + H*	0.03	0.80	-0.04	0.75	0.01	0.79
10	$CH_2CHCOOCH_3$*** + 2* ↔ $CH_2CHCOOCH_2$**** + H*	0.18	0.99	0.08	0.91	0.13	0.97
11	$CH_2CHCOOCH_3$*** + 2* ↔ $CHCHCOOCH_3$**** + H*	0.07	0.87	0.03	0.82	0.05	0.84
12	$CH_2CHCOOCH_3$*** + 1* ↔ CH_2CHCO*** +CH_3O*	0.37	0.91	0.46	0.92	0.41	0.92
13	$CH_3CHCOOCH_2$*** + 2* ↔ $CH_2CHCOOCH_2$**** + H*	-0.28	0.43	-0.33	0.42	-0.32	0.44
14	$CH_3CHCOOCH_2$*** + 3* ↔ CH_3CHCO*** + OCH_2***	-0.24	0.46	-0.15	0.52	-0.21	0.49
15	$CHCHCOOCH_3$**** + 2* ↔ CHCH*** + $COOCH_3$***	-0.10	0.90	-0.02	0.89	-0.06	0.88
16	$CH_2CHCOOCH_2$**** + 3* ↔ CH_2CH*** + $COOCH_2$****	-0.04	0.95	0.07	0.99	0.02	0.97
17	$CH_2CHCOOCH_2$**** + 2* ↔ CH_2CHCO*** + OCH_2***	-0.27	0.41	-0.16	0.44	-0.22	0.43
18	$CH_2CH_2COOCH_3$*** + 1* ↔ $CH_2CHCOOCH_3$*** + H*	-0.61	0.38	-0.62	0.36	-0.61	0.38
19	$CH_2CH_2COOCH_3$*** + 1* ↔ $CH_2CH_2COOCH_2$*** + H*	0.09	0.91	0.00	0.86	0.04	0.90
20	$CH_2CH_2COOCH_3$*** + 2* ↔ CH_2CH_2** + $COOCH_3$***	-0.43	1.03	-0.34	1.04	-0.37	1.04
21	$CH_2CH_2COOCH_3$*** + 1* ↔ CH_2CH_2CO*** + CH_3O*	0.20	0.62	0.33	0.67	0.27	0.66
22	$CH_2CH_2COOCH_2$*** + 1* ↔ $CH_2CHCOOCH_2$**** + H*	-0.52	0.66	-0.54	0.65	-0.52	0.66
23	$CH_2CH_2COOCH_2$*** + 3* ↔ CH_2CH_2** +$COOCH_2$****	-0.63	0.89	-0.50	0.96	-0.55	0.94
24	$CH_2CH_2COOCH_2$*** + 3* ↔ CH_2CH_2CO*** + OCH_2***	-0.37	0.27	-0.24	0.33	-0.29	0.32
25	$CH_3CH_2COOCH_2$*** + 1* ↔ $CH_3CHCOOCH_2$*** + H*	-0.08	0.60	-0.11	0.62	-0.11	0.60
26	$CH_3CH_2COOCH_2$*** + 1* ↔ $CH_2CH_2COOCH_2$*** + H*	0.16	0.96	0.09	0.92	0.09	0.94
27	$CH_3CH_2COOCH_2$*** + 1* ↔ CH_3CH_2COO** + CH_2**	-0.60	0.67	-0.46	0.70	-0.57	0.67
28	$CH_3CH_2COOCH_2$*** + 3* ↔ CH_3CH_2CO*** + OCH_2***	-0.37	0.21	-0.24	0.26	-0.34	0.23
29	CH_3CH_2CO*** + 1* ↔ CH_3CHCO*** + H*	0.05	0.86	-0.01	0.79	0.02	0.85
30	CH_3CH_2CO*** ↔ CH_3CH_2* + CO* + 1*	-0.63	1.02	-0.72	1.01	-0.68	1.03
31	CH_3CHCO*** + 1* ↔ CH_2CHCO*** + H*	-0.31	0.49	-0.35	0.43	-0.33	0.48
32	CH_3CHCO*** ↔ CH_3CH** + CO*	-0.83	0.98	-0.90	0.99	-0.88	0.98
33	CH_3CHCO*** + 1* ↔ CH_3CCO*** + H*	-0.38	0.54	-0.40	0.52	-0.40	0.53
34	CH_2CHCO*** + 1* ↔ CH_2CH*** + CO*	-0.73	0.80	-0.79	0.80	-0.78	0.80
35	CH_2CHCO*** + 2* ↔ $CHCHCO$**** + H*	0.00	0.68	-0.01	0.68	0.00	0.69
36	$CHCHCO$**** ↔ CHCH*** + CO*	-1.11	0.59	-1.16	0.63	-1.16	0.60
37	CH_3CCO*** ↔ CH_3C* + CO* + 1*	-1.41	0.45	-1.47	0.44	-1.46	0.45
38	CH_2CH_2CO*** ↔ CH_2CH_2** + CO*	-1.25	0.73	-1.31	0.72	-1.30	0.71

39	$CH_2CH_2CO^{***} + 1^* \leftrightarrow CH_2CHCO^{***} + H^*$	-0.44	0.69	-0.48	0.66	-0.47	0.68
40	$COOCH_3^{***} + 2^* \leftrightarrow COOCH_2^{***} + H^*$	-0.12	0.64	-0.16	0.61	-0.13	0.64
41	$COOCH_3^{***} \leftrightarrow CO^* + CH_3O^* + 1^*$	-0.62	0.54	-0.65	0.57	-0.65	0.55
42	$COOCH_3^{***} \leftrightarrow CO_2^* + CH_3^* + 1^*$	-0.48	1.48	-0.41	1.40	-0.44	1.46
43	$COOCH_2^{****} \leftrightarrow CO^* + OCH_2^{***}$	-0.96	0.26	-1.02	0.24	-1.02	0.25
44	$COOCH_2^{****} \leftrightarrow CO_2^* + CH_2^{**} + 1^*$	-0.38	0.89	-0.29	0.86	-0.34	0.87
45	$CHCH^{***} + H^* \leftrightarrow CH_2CH^{***} + 1^*$	0.29	0.82	0.31	0.84	0.30	0.83
46	$CH_2CH^{***} \leftrightarrow CH_2C^{**} + H^*$	-0.42	0.45	-0.45	0.44	-0.44	0.44
47	$CH_2C^{**}+H^* \leftrightarrow CH_3C^{**} + 2^*$	-0.27	0.87	-0.24	0.87	-0.26	0.87
48	$CH_2CH^{***} + H^* \leftrightarrow CH_2CH_2^{**} + 2^*$	-0.07	0.87	-0.04	0.87	-0.05	0.88
49	$CH_2CH^{***} + H^* \leftrightarrow CH_3CH^{**} + 2^*$	0.22	0.79	0.23	0.78	0.24	0.79
50	$CH_3C^{***} + H^* \leftrightarrow CH_3CH^{**} + 2^*$	0.96	1.17	0.97	1.17	0.98	1.18
51	$CH_3CH^{**} + H^* \leftrightarrow CH_3CH_2^* + 2^*$	0.15	0.82	0.20	0.84	0.18	0.83
52	$CH_2CH_2^{**} + H^* \leftrightarrow CH_3CH_2^* + 2^*$	-0.44	0.45	-0.42	0.43	-0.43	0.43
53	$CH_3CH_2^* + H^* \leftrightarrow CH_3CH_3^* + 1^*$	-0.03	0.60	-0.02	0.61	-0.03	0.61
54	$CH_3O^* + 3^* \leftrightarrow CH_2O^{***} + H^*$	-0.46	0.47	-0.54	0.43	-0.50	0.46
55	$CH_2O^{***} + 1^* \leftrightarrow CHO^{***} + H^*$	-0.85	0.56	-0.83	0.58	-0.83	0.58
56	$CHO^{***} \leftrightarrow CO^* + H^* + 1^*$	-1.41	0.08	-1.50	0.09	-1.50	0.08
57	$CH_3O^* + H^* \leftrightarrow CH_3OH^* + 1^*$	0.12	0.69	0.02	0.65	0.06	0.68
58	$CH_2^{**} + H^* \leftrightarrow CH_3^* + 2^*$	0.02	0.75	0.04	0.76	0.03	0.76
59	$CH_3^* + H^* \leftrightarrow CH_4^* + 1^*$	-0.15	0.55	-0.12	0.56	-0.13	0.56
60	$CH_3CH_2COO^{**} \leftrightarrow CH_3CH_2^* + CO_2^*$	0.16	1.37	0.20	1.31	0.21	1.35
61	$CH_3CH_2COO^{**} + 2^* \leftrightarrow CH_3CHCOO^{***} + H^*$	0.44	1.28	0.26	1.04	0.39	1.19
62	$CH_3CHCOO^{***} + \leftrightarrow CH_3CH^{**} + CO_2^*$	-0.39	0.92	-0.22	0.97	-0.32	0.94
63	$CH_3CHCOO^{***} + 1^* \leftrightarrow CH_3CCOO^{***} + H^*$	-0.09	0.85	-0.17	0.75	-0.15	0.79
64	$CH_3CCOO^{***} \leftrightarrow CH_3C^* + CO_2^* + 1^*$	-1.22	0.64	-0.99	0.83	-1.11	0.73
65	$CH_3CH_2COOCH_3 + 2^* \leftrightarrow CH_3CH_2COOCH_3^{**}$	0.45	N/A	0.36	N/A	0.31	N/A
66	$CH_3CH_3 + 1^* \leftrightarrow CH_3CH_3^*$	0.62	N/A	0.64	N/A	0.61	N/A
67	$CH_2CH_2 + 2^* \leftrightarrow CH_2CH_2^{**}$	-0.14	N/A	-0.12	N/A	-0.13	N/A
68	$CHCH + 3^* \leftrightarrow CHCH^{***}$	-1.17	N/A	-1.18	N/A	-1.17	N/A
69	$CH_4 + 1^* \leftrightarrow CH_4^*$	0.48	N/A	0.52	N/A	0.50	N/A
70	$CH_3OH + 1^* \leftrightarrow CH_3OH^*$	0.40	N/A	0.33	N/A	0.34	N/A
71	$CO + 1^* \leftrightarrow CO^*$	-1.19	N/A	-1.27	N/A	-1.25	N/A
72	$CO_2 + 1^* \leftrightarrow CO_2^*$	0.52	N/A	0.54	N/A	0.52	N/A
73	$H_2 + 2^* \leftrightarrow 2H^*$	-0.58	N/A	-0.61	N/A	-0.61	N/A

Table 3. Equilibrium and forward rate constants in the vapor phase and in the presence of liquid water and 1,4-dioxane for all elementary reaction steps in the HDO of methyl propionate over a Pd(111) model surface at a temperature of 473 K.

#	Reaction	Gas		Water		1,4-Dioxane	
		K_{eq}	k_f (s^{-1})	K_{eq}	k_f (s^{-1})	K_{eq}	k_f (s^{-1})
1	$CH_3CH_2COOCH_3$** + 1* ↔ CH_3CH_2COO** + CH_3*	1.08×10^{5}	2.08×10^{-4}	4.95×10^{3}	3.03×10^{-4}	4.91×10^{3}	6.46×10^{-5}
2	$CH_3CH_2COOCH_3$** + 2*↔ CH_3CH_2CO*** + CH_3O*	7.63×10^{-3}	3.96×10^{4}	1.20×10^{-4}	2.77×10^{4}	1.69×10^{-4}	3.14×10^{3}
3	$CH_3CH_2COOCH_3$** + 2* ↔ $CH_3CHCOOCH_3$*** + H*	1.52	1.37×10^{5}	1.58	1.31×10^{5}	2.66×10^{-1}	2.04×10^{4}
4	$CH_3CH_2COOCH_3$** + 2* ↔ $CH_2CH_2COOCH_3$*** + H*	1.91×10^{-2}	1.01×10^{4}	2.89×10^{-2}	2.80×10^{4}	4.06×10^{-3}	2.95×10^{3}
5	$CH_3CH_2COOCH_3$** + 2* ↔ $CH_3CH_2COOCH_2$*** + H*	9.81×10^{-2}	5.02×10^{4}	2.77×10^{-1}	1.03×10^{5}	1.50×10^{-2}	1.11×10^{4}
6	$CH_3CHCOOCH_3$*** + 1* ↔ CH_3CHCOO*** + CH_3*	2.41	4.00×10^{-5}	7.54	1.61×10^{-4}	2.16	6.64×10^{-5}
7	$CH_3CHCOOCH_3$*** + 1* ↔ CH_3CHCO*** + CH_3O*	2.49×10^{-3}	1.30×10^{5}	1.73×10^{-4}	3.00×10^{4}	5.82×10^{-4}	5.10×10^{4}
8	$CH_3CHCOOCH_3$*** + 1* ↔ $CH_2CHCOOCH_3$*** + H*	3.98×10^{4}	4.64×10^{7}	7.06×10^{4}	1.11×10^{8}	4.66×10^{4}	6.20×10^{7}
9	$CH_3CHCOOCH_3$*** + 1* ↔ $CH_3CHCOOCH_2$*** + H*	4.89×10^{-1}	3.04×10^{4}	2.55	1.07×10^{5}	7.52×10^{-1}	3.45×10^{4}
10	$CH_2CHCOOCH_3$*** + 2* ↔ $CH_2CHCOOCH_2$**** +H*	1.27×10^{-2}	2.69×10^{2}	1.31×10^{-1}	1.84×10^{3}	4.48×10^{-2}	5.09×10^{2}
11	$CH_2CHCOOCH_3$*** + 2* ↔ $CHCHCOOCH_3$**** + H*	1.90×10^{-1}	5.29×10^{3}	4.75×10^{-1}	1.99×10^{4}	3.26×10^{-1}	1.07×10^{4}
12	$CH_2CHCOOCH_3$*** + 1* ↔ CH_2CHCO*** + CH_3O*	1.28×10^{-4}	1.98×10^{3}	1.25×10^{-5}	1.44×10^{3}	4.38×10^{-5}	1.46×10^{3}
13	$CH_3CHCOOCH_2$*** + 2* ↔ $CH_2CHCOOCH_2$**** +H*	1.03×10^{3}	2.69×10^{8}	3.62×10^{3}	3.52×10^{8}	2.77×10^{3}	2.20×10^{8}
14	$CH_3CHCOOCH_2$*** + 3* ↔ CH_3CHCO*** + OCH_2***	3.77×10^{2}	1.10×10^{8}	3.75×10^{1}	3.19×10^{7}	1.84×10^{2}	6.58×10^{7}
15	$CHCHCOOCH_3$**** + 2* ↔ $CHCH$*** + $COOCH_3$***	1.24×10^{1}	2.77×10^{3}	1.75	2.89×10^{3}	4.92	3.98×10^{3}
16	$CH_2CHCOOCH_2$****+3* ↔ CH_2CH***+$COOCH_2$****	2.59	6.95×10^{2}	1.61×10^{-1}	2.95×10^{2}	6.20×10^{-1}	4.66×10^{2}
17	$CH_2CHCOOCH_2$**** +2* ↔ CH_2CHCO*** +OCH_2***	7.51×10^{2}	3.84×10^{8}	5.29×10^{1}	2.08×10^{8}	2.33×10^{2}	2.78×10^{8}
18	$CH_2CH_2COOCH_3$*** + 1* ↔ $CH_2CHCOOCH_3$*** + H*	3.17×10^{6}	8.55×10^{8}	3.85×10^{6}	1.59×10^{9}	3.06×10^{6}	8.40×10^{8}
19	$CH_2CH_2COOCH_3$*** +1* ↔ $CH_2CH_2COOCH_2$*** +H*	1.14×10^{-1}	1.93×10^{3}	9.67×10^{-1}	6.45×10^{3}	3.62×10^{-1}	2.83×10^{3}
20	$CH_2CH_2COOCH_3$*** + 2* ↔ CH_2CH_2** +$COOCH_3$***	3.87×10^{4}	9.87×10^{1}	3.80×10^{3}	8.60×10^{1}	9.87×10^{3}	7.51×10^{1}
21	$CH_2CH_2COOCH_3$*** + 1* ↔ CH_2CH_2CO*** + CH_3O*	7.44×10^{-3}	2.41×10^{6}	3.30×10^{-4}	6.42×10^{5}	1.18×10^{-3}	1.03×10^{6}
22	$CH_2CH_2COOCH_2$*** +1* ↔ $CH_2CHCOOCH_2$**** +H*	3.52×10^{5}	8.95×10^{5}	5.22×10^{5}	1.07×10^{6}	3.78×10^{5}	9.89×10^{5}
23	$CH_2CH_2COOCH_2$*** +3* ↔ CH_2CH_2**+$COOCH_2$****	5.74×10^{6}	3.30×10^{3}	2.18×10^{5}	5.81×10^{2}	7.25×10^{5}	1.07×10^{3}
24	$CH_2CH_2COOCH_2$*** +3* ↔ CH_2CH_2CO***+OCH_2***	8.44×10^{3}	1.18×10^{10}	3.30×10^{2}	2.90×10^{9}	1.35×10^{3}	4.01×10^{9}
25	$CH_3CH_2COOCH_2$*** + 1* ↔ $CH_3CHCOOCH_2$*** + H*	7.56	3.86×10^{6}	1.46×10^{1}	2.29×10^{6}	1.33×10^{1}	3.58×10^{6}
26	$CH_3CH_2COOCH_2$*** +1* ↔ $CH_2CH_2COOCH_2$*** +H*	2.22×10^{-2}	5.89×10^{2}	1.01×10^{-1}	1.66×10^{3}	9.78×10^{-2}	1.03×10^{3}

27	$CH_3CH_2COOCH_2$*** + 1* ↔ CH_3CH_2COO** + CH_2**	2.74×10^{6}	7.28×10^{5}	7.46×10^{4}	3.13×10^{5}	1.16×10^{6}	7.94×10^{5}
28	$CH_3CH_2COOCH_2$*** +3* ↔ CH_3CH_2CO***+OCH_2***	8.01×10^{3}	5.37×10^{10}	3.32×10^{2}	1.81×10^{10}	3.72×10^{3}	3.49×10^{10}
29	CH_3CH_2CO*** + 1* ↔ CH_3CHCO*** + H*	3.08×10^{-1}	7.47×10^{3}	1.42	3.77×10^{4}	5.72×10^{-1}	8.50×10^{3}
30	CH_3CH_2CO*** ↔ CH_3CH_2* + CO* + 1*	4.73×10^{6}	1.36×10^{2}	4.63×10^{7}	1.54×10^{2}	1.75×10^{7}	9.26×10^{1}
31	CH_3CHCO*** + 1* ↔ CH_2CHCO*** + H*	2.06×10^{3}	5.51×10^{7}	5.10×10^{3}	2.42×10^{8}	3.50×10^{3}	8.45×10^{7}
32	CH_3CHCO*** ↔ CH_3CH** + CO*	6.68×10^{8}	3.55×10^{2}	4.13×10^{9}	2.89×10^{2}	2.35×10^{9}	3.52×10^{2}
33	CH_3CHCO*** + 1* ↔ CH_3CCO*** + H*	1.05×10^{4}	1.68×10^{7}	2.02×10^{4}	2.77×10^{7}	1.79×10^{4}	2.08×10^{7}
34	CH_2CHCO*** + 1* ↔ CH_2CH*** + CO*	6.37×10^{7}	3.06×10^{4}	2.35×10^{8}	3.17×10^{4}	2.15×10^{8}	2.91×10^{4}
35	CH_2CHCO*** + 2* ↔ $CHCHCO$**** + H*	9.03×10^{-1}	5.54×10^{5}	1.44	5.74×10^{5}	1.03	4.66×10^{5}
36	$CHCHCO$**** ↔ $CHCH$*** + CO*	7.59×10^{11}	5.57×10^{6}	2.52×10^{12}	1.96×10^{6}	2.27×10^{12}	3.92×10^{6}
37	CH_3CCO*** ↔ CH_3C* + CO* + 1*	1.00×10^{15}	1.76×10^{8}	4.40×10^{15}	2.03×10^{8}	3.53×10^{15}	1.48×10^{8}
38	CH_2CH_2CO*** ↔ CH_2CH_2** + CO*	2.19×10^{13}	1.81×10^{5}	8.90×10^{13}	1.95×10^{5}	7.55×10^{13}	2.41×10^{5}
39	CH_2CH_2CO*** + 1* ↔ CH_2CHCO*** + H*	5.46×10^{4}	3.89×10^{5}	1.46×10^{5}	9.30×10^{5}	1.14×10^{5}	5.46×10^{5}
40	$COOCH_3$*** + 2* ↔ $COOCH_2$*** + H*	1.69×10^{1}	1.42×10^{6}	5.55×10^{1}	3.06×10^{6}	2.66×10^{1}	1.49×10^{6}
41	$COOCH_3$*** ↔ CO* + CH_3O* + 1*	4.20×10^{6}	1.77×10^{7}	7.73×10^{6}	9.10×10^{6}	9.02×10^{6}	1.29×10^{7}
42	$COOCH_3$*** ↔ CO_2* + CH_3* + 1*	1.21×10^{5}	1.87×10^{-3}	2.60×10^{4}	1.24×10^{-2}	5.35×10^{4}	2.83×10^{-3}
43	$COOCH_2$**** ↔ CO* + OCH_2***	1.85×10^{10}	1.75×10^{10}	7.71×10^{10}	2.58×10^{10}	8.07×10^{10}	2.33×10^{10}
44	$COOCH_2$**** ↔ CO_2* + CH_2** + 1*	1.11×10^{4}	3.62×10^{3}	1.22×10^{3}	6.98×10^{3}	4.46×10^{3}	5.87×10^{3}
45	$CHCH$*** + H* ↔ CH_2CH*** + 1*	8.26×10^{-4}	2.03×10^{4}	4.58×10^{-4}	1.12×10^{4}	6.51×10^{-4}	1.42×10^{4}
46	CH_2CH*** ↔ CH_2C** + H*	3.07×10^{4}	1.73×10^{8}	5.72×10^{4}	2.11×10^{8}	4.55×10^{4}	2.09×10^{8}
47	CH_2C**+H* ↔ CH_3C** + 2*	8.27×10^{2}	5.44×10^{3}	4.07×10^{2}	5.81×10^{3}	1.23×10^{3}	6.58×10^{3}
48	CH_2CH*** + H* ↔ CH_2CH_2** + 2*	6.28	5.64×10^{3}	2.59	5.62×10^{3}	3.09	4.43×10^{3}
49	CH_2CH*** + H* ↔ CH_3CH** + 2*	5.10×10^{-3}	3.71×10^{4}	3.44×10^{-3}	4.77×10^{4}	3.12×10^{-3}	4.16×10^{4}
50	CH_3C*** + H* ↔ CH_3CH** + 2*	6.32×10^{-11}	3.50	4.64×10^{-11}	3.22	3.70×10^{-11}	2.41
51	CH_3CH** + H* ↔ CH_3CH_2* + 2*	2.30×10^{-2}	1.74×10^{4}	7.89×10^{-3}	1.25×10^{4}	1.30×10^{-2}	1.48×10^{4}
52	CH_2CH_2** + H* ↔ CH_3CH_2* + 2*	2.05×10^{-5}	3.54×10^{3}	3.65×10^{-5}	1.05×10^{4}	2.91×10^{-5}	6.67×10^{3}
53	CH_3CH_2* + H* ↔ CH_3CH_3* + 1*	2.18	3.67×10^{6}	1.82	3.24×10^{6}	2.34	3.40×10^{6}
54	CH_3O* + 3* ↔ CH_2O*** + H*	7.42×10^{4}	1.02×10^{8}	5.54×10^{5}	2.55×10^{8}	2.38×10^{5}	1.10×10^{8}
55	CH_2O*** + 1* ↔ CHO*** + H*	1.20×10^{9}	9.66×10^{6}	6.98×10^{8}	6.93×10^{6}	7.44×10^{8}	6.03×10^{6}
56	CHO*** ↔ CO* + H* + 1*	9.35×10^{14}	1.24×10^{12}	1.05×10^{16}	1.01×10^{12}	8.78×10^{15}	1.33×10^{12}
57	CH_3O* + H* ↔ CH_3OH* + 1*	5.74×10^{-2}	4.23×10^{5}	6.35×10^{-1}	1.06×10^{6}	2.38×10^{-1}	5.54×10^{5}

58	CH_2** + H* ↔ CH_3* + 2*	6.45×10^{-1}	1.12×10^{5}	3.84×10^{-1}	8.14×10^{4}	4.51×10^{-1}	8.29×10^{4}
59	CH_3* + H* ↔ CH_4* + 1*	4.38×10^{1}	1.50×10^{7}	2.07×10^{1}	9.54×10^{6}	2.74×10^{1}	9.98×10^{6}
60	CH_3CH_2COO** ↔ CH_3CH_2* + CO_2*	1.75×10^{-2}	2.49×10^{-2}	6.83×10^{-3}	1.21×10^{-1}	6.49×10^{-3}	3.82×10^{-2}
61	CH_3CH_2COO** + 2* ↔ CH_3CHCOO*** + H*	2.14×10^{-5}	2.46×10^{-1}	1.52×10^{-3}	9.06×10^{1}	7.41×10^{-5}	2.12
62	CH_3CHCOO*** ↔ CH_3CH** + CO_2*	1.50×10^{4}	1.41×10^{3}	2.40×10^{2}	4.14×10^{2}	2.84×10^{3}	9.04×10^{2}
63	CH_3CHCOO*** + 1* ↔ CH_3CCOO*** + H*	8.51	7.97×10^{3}	5.93×10^{1}	1.02×10^{5}	3.94×10^{1}	3.67×10^{4}
64	CH_3CCOO*** ↔ CH_3C* + CO_2* + 1*	1.04×10^{13}	1.65×10^{6}	3.24×10^{10}	1.51×10^{4}	7.24×10^{11}	1.65×10^{5}
65	$CH_3CH_2COOCH_3$ + 2* ↔ $CH_3CH_2COOCH_3$**	1.81×10^{-5}	8.73×10^{7}	1.50×10^{-4}	8.73×10^{7}	5.61×10^{-4}	8.73×10^{7}
66	CH_3CH_3 + 1* ↔ CH_3CH_3*	2.79×10^{-7}	1.50×10^{8}	1.49×10^{-7}	1.50×10^{8}	3.03×10^{-7}	1.50×10^{8}
67	CH_2CH_2 + 2* ↔ CH_2CH_2**	2.79×10^{1}	1.55×10^{8}	2.01×10^{1}	1.55×10^{8}	2.47×10^{1}	1.55×10^{8}
68	CHCH + 3* ↔ CHCH***	2.59×10^{12}	1.61×10^{8}	3.76×10^{12}	1.61×10^{8}	2.65×10^{12}	1.61×10^{8}
69	CH_4 + 1* ↔ CH_4*	8.51×10^{-6}	2.05×10^{8}	2.88×10^{-6}	2.05×10^{8}	4.82×10^{-6}	2.05×10^{8}
70	CH_3OH + 1* ↔ CH_3OH*	5.89×10^{-5}	1.45×10^{8}	3.36×10^{-4}	1.45×10^{8}	2.38×10^{-4}	1.45×10^{8}
71	CO + 1* ↔ CO*	5.33×10^{12}	1.55×10^{8}	3.87×10^{13}	1.55×10^{8}	2.64×10^{13}	1.55×10^{8}
72	CO_2 + 1* ↔ CO_2*	2.79×10^{-6}	1.24×10^{8}	1.69×10^{-6}	1.24×10^{8}	3.04×10^{-6}	1.24×10^{8}
73	H_2 + 2* → 2H*	1.65×10^{6}	5.80×10^{8}	3.05×10^{6}	5.80×10^{8}	3.14×10^{6}	5.80×10^{8}

Table 4. Calculated net rate (turnover frequency) in the gas and liquid phase for all elementary steps in the HDO of methyl propionate over a Pd(111) model surface at a temperature of 473 K.

#	Reaction	Gas	Water	1,4-Dioxane
		TOF (s^{-1})	TOF (s^{-1})	TOF (s^{-1})
1	$CH_3CH_2COOCH_3$** + 1* ↔ CH_3CH_2COO** + CH_3*	6.16×10^{-15}	2.39×10^{-15}	1.39×10^{-14}
2	$CH_3CH_2COOCH_3$** + 2*↔ CH_3CH_2CO*** + CH_3O*	6.43×10^{-8}	3.79×10^{-9}	2.94×10^{-8}
3	$CH_3CH_2COOCH_3$** + 2* ↔ $CH_3CHCOOCH_3$*** + H*	1.85×10^{-7}	6.94×10^{-9}	1.46×10^{-7}
4	$CH_3CH_2COOCH_3$** + 2* ↔ $CH_2CH_2COOCH_3$*** + H*	1.39×10^{-8}	1.50×10^{-9}	2.12×10^{-8}
5	$CH_3CH_2COOCH_3$** + 2* ↔ $CH_3CH_2COOCH_2$*** + H*	7.84×10^{-8}	4.21×10^{-9}	8.93×10^{-8}
6	$CH_3CHCOOCH_3$*** + 1* ↔ CH_3CHCOO*** + CH_3*	1.34×10^{-18}	5.31×10^{-19}	2.55×10^{-18}
7	$CH_3CHCOOCH_3$*** + 1* ↔ CH_3CHCO*** + CH_3O*	4.35×10^{-9}	9.90×10^{-11}	1.96×10^{-9}
8	$CH_3CHCOOCH_3$*** + 1* ↔ $CH_2CHCOOCH_3$*** + H*	1.80×10^{-7}	6.79×10^{-9}	1.43×10^{-7}
9	$CH_3CHCOOCH_3$*** + 1* ↔ $CH_3CHCOOCH_2$*** + H*	9.01×10^{-10}	5.91×10^{-11}	1.01×10^{-9}
10	$CH_2CHCOOCH_3$*** + 2* ↔ $CH_2CHCOOCH_2$**** +H*	1.39×10^{-9}	9.37×10^{-11}	2.36×10^{-9}
11	$CH_2CHCOOCH_3$*** + 2* ↔ $CHCHCOOCH_3$**** + H*	1.25×10^{-11}	5.84×10^{-14}	1.77×10^{-11}
12	$CH_2CHCOOCH_3$*** + 1* ↔ CH_2CHCO*** + CH_3O*	1.91×10^{-7}	8.15×10^{-9}	1.61×10^{-7}
13	$CH_3CHCOOCH_2$*** + 2* ↔ $CH_2CHCOOCH_2$**** +H*	1.76×10^{-9}	4.62×10^{-10}	3.73×10^{-9}
14	$CH_3CHCOOCH_2$*** + 3* ↔ CH_3CHCO*** + OCH_2***	4.99×10^{-11}	1.67×10^{-12}	5.64×10^{-11}
15	$CHCHCOOCH_3$**** + 2* ↔ CHCH*** + $COOCH_3$***	1.25×10^{-11}	5.84×10^{-14}	1.77×10^{-11}
16	$CH_2CHCOOCH_2$****+3* ↔ CH_2CH***+$COOCH_2$****	3.12×10^{-16}	1.37×10^{-17}	4.44×10^{-16}
17	$CH_2CHCOOCH_2$**** +2* ↔ CH_2CHCO*** +OCH_2***	3.14×10^{-9}	5.56×10^{-10}	6.08×10^{-9}
18	$CH_2CH_2COOCH_3$*** + 1* ↔ $CH_2CHCOOCH_3$*** + H*	1.30×10^{-8}	1.46×10^{-9}	2.06×10^{-8}
19	$CH_2CH_2COOCH_3$*** +1* ↔ $CH_2CH_2COOCH_2$*** +H*	7.41×10^{-13}	1.66×10^{-13}	1.58×10^{-12}
20	$CH_2CH_2COOCH_3$*** +2* ↔ CH_2CH_2** + $COOCH_3$***	2.09×10^{-15}	8.92×10^{-17}	1.88×10^{-15}
21	$CH_2CH_2COOCH_3$*** + 1* ↔ CH_2CH_2CO*** + CH_3O*	9.33×10^{-10}	3.84×10^{-11}	5.93×10^{-10}
22	$CH_2CH_2COOCH_2$*** +1* ↔ $CH_2CHCOOCH_2$**** +H*	-3.22×10^{-15}	2.53×10^{-15}	-3.88×10^{-15}
23	$CH_2CH_2COOCH_2$*** +3* ↔ CH_2CH_2**+$COOCH_2$****	2.85×10^{-19}	1.43×10^{-19}	7.63×10^{-19}
24	$CH_2CH_2COOCH_2$***+3* ↔ CH_2CH_2CO*** +OCH_2***	1.02×10^{-12}	7.16×10^{-13}	2.86×10^{-12}
25	$CH_3CH_2COOCH_2$*** + 1* ↔ $CH_3CHCOOCH_2$*** + H*	9.07×10^{-10}	4.05×10^{-10}	2.78×10^{-9}
26	$CH_3CH_2COOCH_2$*** +1* ↔ $CH_2CH_2COOCH_2$*** +H*	2.73×10^{-13}	5.52×10^{-13}	1.27×10^{-12}
27	$CH_3CH_2COOCH_2$*** + 1* ↔ CH_3CH_2COO** + CH_2**	3.49×10^{-10}	2.07×10^{-10}	1.03×10^{-9}
28	$CH_3CH_2COOCH_2$*** +3* ↔ CH_3CH_2CO***+OCH_2***	7.71×10^{-8}	3.60×10^{-9}	8.54×10^{-8}
29	CH_3CH_2CO*** + 1* ↔ CH_3CHCO*** + H*	1.05×10^{-7}	5.88×10^{-9}	9.15×10^{-8}
30	CH_3CH_2CO*** ↔ CH_3CH_2* + CO* + 1*	3.60×10^{-8}	1.50×10^{-9}	2.33×10^{-8}
31	CH_3CHCO*** + 1* ↔ CH_2CHCO*** + H*	-6.40×10^{-8}	-6.98×10^{-9}	-6.09×10^{-8}
32	CH_3CHCO*** ↔ CH_3CH** + CO*	6.71×10^{-11}	7.78×10^{-12}	6.00×10^{-11}
33	CH_3CHCO*** + 1* ↔ CH_3CCO*** + H*	1.74×10^{-7}	1.30×10^{-8}	1.54×10^{-7}
34	CH_2CHCO*** + 1* ↔ CH_2CH*** + CO*	5.95×10^{-8}	1.99×10^{-9}	5.45×10^{-8}
35	CH_2CHCO*** + 2* ↔ $CHCHCO$**** + H*	5.89×10^{-8}	-2.76×10^{-10}	3.79×10^{-8}
36	$CHCHCO$**** ↔ CHCH*** + CO*	5.89×10^{-8}	-2.76×10^{-10}	3.79×10^{-8}
37	CH_3CCO*** ↔ CH_3C* + CO* + 1*	1.74×10^{-7}	1.30×10^{-8}	1.54×10^{-7}

38	$CH_2CH_2CO^{***} \leftrightarrow CH_2CH_2^{**} + CO^*$	9.86×10^{-10}	5.09×10^{-11}	6.67×10^{-10}
39	$CH_2CH_2CO^{***} + 1^* \leftrightarrow CH_2CHCO^{***} + H^*$	-5.23×10^{-11}	-1.19×10^{-11}	-7.15×10^{-11}
40	$COOCH_3^{***} + 2^* \leftrightarrow COOCH_2^{***} + H^*$	3.02×10^{-15}	9.22×10^{-18}	3.87×10^{-15}
41	$COOCH_3^{***} \leftrightarrow CO^* + CH_3O^* + 1^*$	1.25×10^{-11}	9.09×10^{-14}	1.77×10^{-11}
42	$COOCH_3^{***} \leftrightarrow CO_2^* + CH_3^* + 1^*$	1.33×10^{-21}	1.24×10^{-22}	3.89×10^{-21}
43	$COOCH_2^{****} \leftrightarrow CO^* + OCH_2^{***}$	3.31×10^{-15}	-9.49×10^{-17}	4.32×10^{-15}
44	$COOCH_2^{****} \leftrightarrow CO_2^* + CH_2^{**} + 1^*$	7.88×10^{-21}	5.55×10^{-22}	6.81×10^{-21}
45	$CHCH^{***} + H^* \leftrightarrow CH_2CH^{***} + 1^*$	5.90×10^{-8}	-2.76×10^{-10}	3.79×10^{-8}
46	$CH_2CH^{***} \leftrightarrow CH_2C^{**} + H^*$	-2.98×10^{-7}	-1.42×10^{-8}	-1.99×10^{-7}
47	$CH_2C^{**} + H^* \leftrightarrow CH_3C^{**} + 2^*$	-2.98×10^{-7}	-1.42×10^{-8}	-1.99×10^{-7}
48	$CH_2CH^{***} + H^* \leftrightarrow CH_2CH_2^{**} + 2^*$	3.28×10^{-8}	5.03×10^{-9}	3.27×10^{-8}
49	$CH_2CH^{***} + H^* \leftrightarrow CH_3CH^{**} + 2^*$	3.83×10^{-7}	1.09×10^{-8}	2.59×10^{-7}
50	$CH_3C^{***} + H^* \leftrightarrow CH_3CH^{**} + 2^*$	-1.12×10^{-7}	-1.26×10^{-9}	-6.17×10^{-9}
51	$CH_3CH^{**} + H^* \leftrightarrow CH_3CH_2^* + 2^*$	2.72×10^{-7}	9.65×10^{-9}	2.53×10^{-7}
52	$CH_2CH_2^{**} + H^* \leftrightarrow CH_3CH_2^* + 2^*$	3.22×10^{-8}	4.89×10^{-9}	8.20×10^{-9}
53	$CH_3CH_2^* + H^* \leftrightarrow CH_3CH_3^* + 1^*$	3.40×10^{-7}	1.63×10^{-8}	2.85×10^{-7}
54	$CH_3O^* + 3^* \leftrightarrow CH_2O^{***} + H^*$	1.44×10^{-8}	1.06×10^{-11}	4.53×10^{-9}
55	$CH_2O^{***} + 1^* \leftrightarrow CHO^{***} + H^*$	9.47×10^{-8}	4.17×10^{-9}	9.61×10^{-8}
56	$CHO^{***} \leftrightarrow CO^* + H^* + 1^*$`	9.47×10^{-8}	4.17×10^{-9}	9.61×10^{-8}
57	$CH_3O^* + H^* \leftrightarrow CH_3OH^* + 1^*$	2.47×10^{-7}	1.21×10^{-8}	1.89×10^{-7}
58	$CH_2^{**} + H^* \leftrightarrow CH_3^* + 2^*$	3.49×10^{-10}	2.07×10^{-10}	1.03×10^{-9}
59	$CH_3^* + H^* \leftrightarrow CH_4^* + 1^*$	3.49×10^{-10}	2.07×10^{-10}	1.03×10^{-9}
60	$CH_3CH_2COO^{**} \leftrightarrow CH_3CH_2^* + CO_2^*$	3.47×10^{-10}	2.04×10^{-10}	1.02×10^{-9}
61	$CH_3CH_2COO^{**} + 2^* \leftrightarrow CH_3CHCOO^{***} + H^*$	1.99×10^{-12}	2.18×10^{-12}	1.24×10^{-11}
62	$CH_3CHCOO^{***} \leftrightarrow CH_3CH^{**} + CO_2^*$	1.52×10^{-12}	4.39×10^{-13}	4.49×10^{-12}
63	$CH_3CHCOO^{***} + 1^* \leftrightarrow CH_3CCOO^{***} + H^*$	4.71×10^{-13}	1.74×10^{-12}	7.90×10^{-12}
64	$CH_3CCOO^{***} \leftrightarrow CH_3C^* + CO_2^* + 1^*$	4.71×10^{-13}	1.74×10^{-12}	7.90×10^{-12}
65	$CH_3CH_2COOCH_3 + 2^* \leftrightarrow CH_3CH_2COOCH_3^{**}$	3.42×10^{-7}	1.64×10^{-8}	2.86×10^{-7}
66	$CH_3CH_3 + 1^* \leftrightarrow CH_3CH_3^*$	3.40×10^{-7}	1.63×10^{-8}	2.85×10^{-7}
67	$CH_2CH_2 + 2^* \leftrightarrow CH_2CH_2^{**}$	1.56×10^{-9}	1.89×10^{-10}	3.39×10^{-10}
68	$CHCH + 3^* \leftrightarrow CHCH^{***}$	5.29×10^{-14}	3.08×10^{-15}	1.53×10^{-15}
69	$CH_4 + 1^* \leftrightarrow CH_4^*$	3.49×10^{-10}	2.07×10^{-10}	1.03×10^{-9}
70	$CH_3OH + 1^* \leftrightarrow CH_3OH^*$	2.47×10^{-7}	1.21×10^{-8}	1.89×10^{-7}
71	$CO + 1^* \leftrightarrow CO^*$	Equilibrium	Equilibrium	Equilibrium
72	$CO_2 + 1^* \leftrightarrow CO_2^*$	3.49×10^{-10}	2.07×10^{-10}	1.03×10^{-9}
73	$H_2 + 2^* \rightarrow 2H^*$	Equilibrium	Equilibrium	Equilibrium

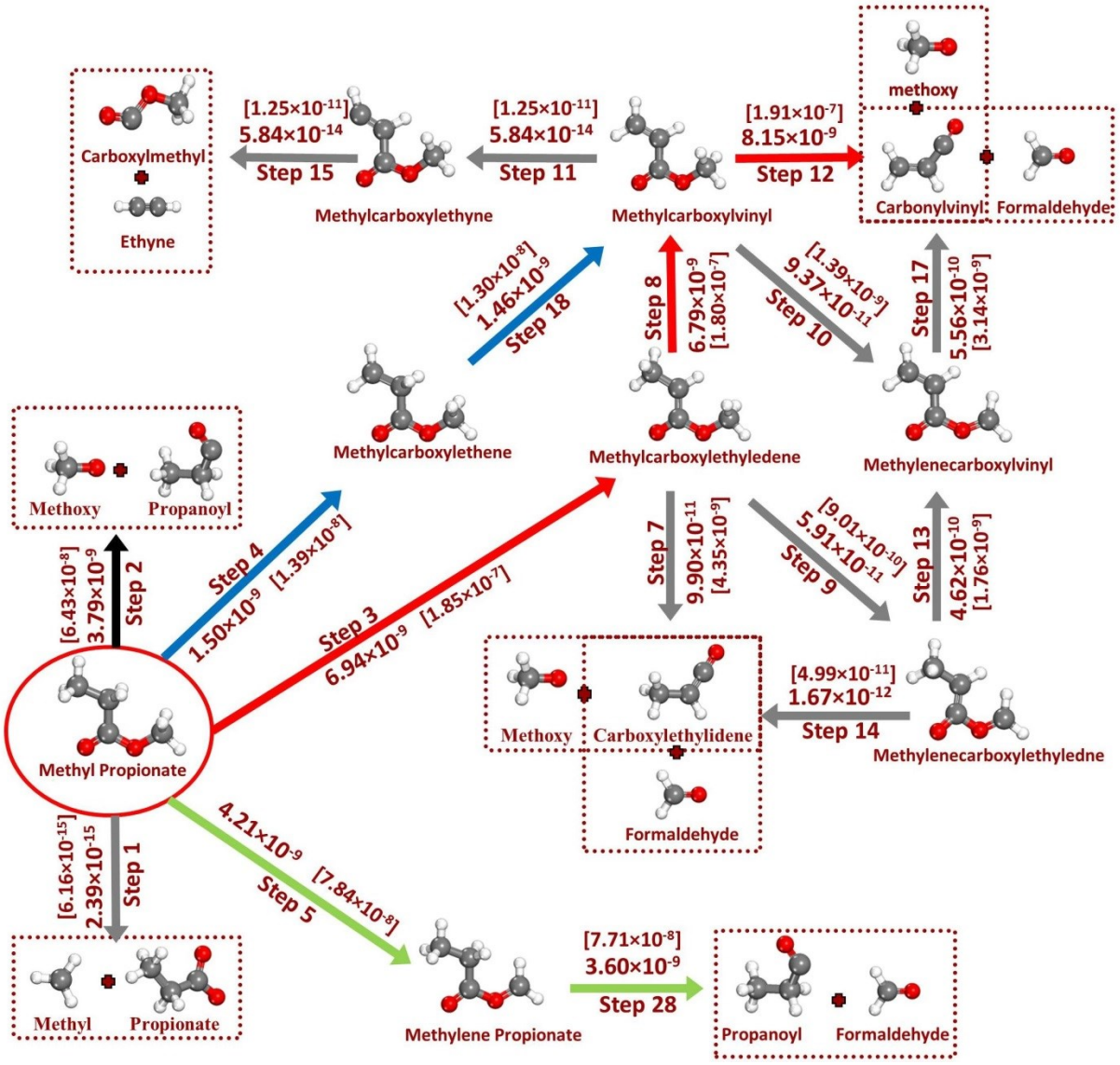

Figure 1. Schematic representation of the most important reaction pathways in the network considered in the HDO of methyl propionate over Pd (111) in the presence of water. We note that in our microkinetic calculations, we included all the elementary steps illustrated in Table 1; however, this Figure is a schematic of elementary steps involved in the dominant pathways of the HDO of methyl propionate. TOFs (s^{-1}) shown for various elementary steps are computed at a temperature of 473 K, a methyl propionate gas phase pressure of 0.01 bar and a hydrogen partial pressure of 0.2 bar. For convenience in comparison, the calculated values of TOFs (s^{-1}) in the absence of solvent are shown in [ ] next to the obtained values of TOFs(s^{-1}) in the presence of water. TOFs (s^{-1}) for elementary reactions not shown in this figure are illustrated in Table 4. The most dominant pathway is shown in red color ($CH_3CH_2COOCH_3$→$CH_3CHCOOCH_3$→$CH_2CHCOOCH_3$→$CH_2CHCO+OCH_3$→…→$CH_3CH_3+CO+CH_3OH$). Other competitive pathways are shown in black, blue, and green.

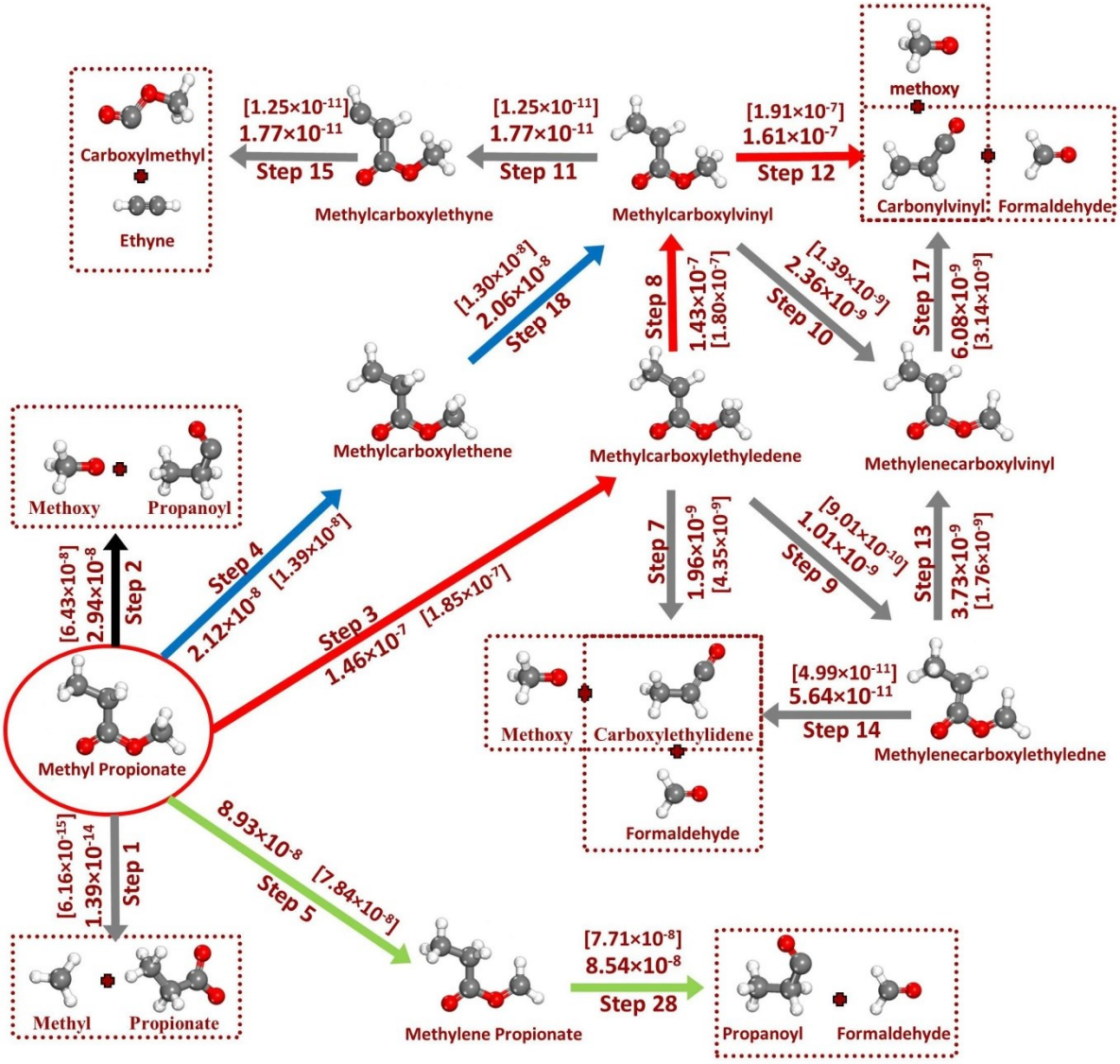

Figure 2. Schematic representation of the most important reaction pathways in the network considered in the HDO of methyl propionate over Pd (111) in the presence of 1,4-dioxane. We note that in our microkinetic calculations, we included all the elementary steps illustrated in Table 1; however, this Figure is a schematic of elementary steps involved in the dominant pathways of the HDO of methyl propionate. TOFs (s^{-1}) shown for various elementary steps are computed at a temperature of 473 K, a methyl propionate gas phase pressure of 0.01 bar and a hydrogen partial pressure of 0.2 bar. For convenience in comparison, the calculated values of TOFs (s^{-1}) in the absence of solvent are shown in [ ] next to the obtained values of TOFs(s^{-1}) in the presence of 1,4-dioxane. TOFs (s^{-1}) for elementary reactions not shown in this figure are illustrated in Table 4. The most dominant pathway is shown in red color ($CH_3CH_2COOCH_3$→$CH_3CHCOOCH_3$→$CH_2CHCOOCH_3$→$CH_2CHCO+OCH_3$→…→$CH_3CH_3+CO+CH_3OH$). Other competitive pathways are shown in black, blue, and green.